



Poly(styrene-co-maleic acid)-mediated isolation of supramolecular membrane protein complexes from plant thylakoids

Olena I. Korotych^a, Thao T. Nguyen^{a,1}, Brandon C. Reagan^a, Tessa M. Burch-Smith^a, Barry D. Bruce^{a,b,*}

^a Department of Biochemistry & Cellular and Molecular Biology, University of Tennessee at Knoxville, TN 37996, United States of America

^b Department of Chemical and Biomolecular Engineering, University of Tennessee at Knoxville, TN 37996, United States of America

ARTICLE INFO

Keywords:

Membrane protein extraction
Photosystem II
Light-harvesting complex (antenna complex)
Styrene-maleic acid (SMA) copolymer
Styrene-maleic acid lipoparticle (SMALP)
Plant thylakoid membrane (TM)

ABSTRACT

Derivatives of poly(styrene-co-maleic acid) (pSMA), have recently emerged as effective reagents for extracting membrane protein complexes from biological membranes. Despite recent progress in using SMAs to study artificial and bacterial membranes, very few reports have addressed their use in studying the highly abundant and well characterized thylakoid membranes. Recently, we tested the ability of twelve commercially available SMA copolymers with different physicochemical properties to extract membrane protein complexes (MPCs) from spinach thylakoid membrane. Based on the efficacy of both protein and chlorophyll extraction, we have found five highly efficient SMA copolymers: SMA® 1440, XIRAN® 25010, XIRAN® 30010, SMA® 17352, and SMA® PRO 10235, that show promise in extracting MPCs from chloroplast thylakoids. To further advance the application of these polymers for studying biomembrane organization, we have examined the composition of thylakoid supramolecular protein complexes extracted by the five SMA polymers mentioned above. Two commonly studied plants, spinach (*Spinacia oleracea*) and pea (*Pisum sativum*), were used for extraction as model biomembranes. We found that the pSMAs differentially extract protein complexes from spinach and pea thylakoids. Based on their differential activity, which correlates with the polymer chemical structure, pSMAs can be divided into two groups: unfunctionalized polymers and ester derivatives.

1. Introduction

Compared to soluble proteins, the functional and structural characterization of membrane protein complexes (MPCs) still remains a challenge [1,2]. This is mostly due to the difficulties in establishing experimental conditions under which the proteins of interest can be

isolated from biological membranes in their native conformations and lipid environments. About a decade ago researchers began using surface-active polymers [3], particularly poly(styrene-co-maleic acid) salts (pSMA-S), to solubilize lipid membranes and extract membrane proteins [4–7] as an alternative to traditionally used detergents. Since then there has been steady progress in the application of SMA copolymers for

Abbreviations: ANOVA, analysis of variance; APS, ammonium persulfate; BCA, bicinchoninic acid; BDB, Barry D. Bruce; bis-tris, bis(2-hydroxyethyl)amino-tris (hydroxymethyl)methane; BSA, bovine serum albumin; CBB, Coomassie brilliant blue; cps, counts per second; DDM, β , n -dodecyl- β -D-maltoside; DGDG, digalactosyldiacylglycerol; DTT, dithiothreitol; EDC, 1-ethyl-3-(3-dimethylaminopropyl)carbodiimide; EGC, Environmental Growth Chamber; FI, fluorescence intensity; GKB, glycine-KOH buffer; GKRB, glycine-KOH resuspending buffer; GKSB, glycine-KOH solubilizing buffer; HDF, high-density fraction; HEPES, 4-(2-hydroxyethyl)-1-piperazineethanesulfonic acid; IgG, immunoglobulin G; IgY, immunoglobulin Y; IHD, index of hydrogen deficiency; LDS, lithium dodecyl sulfate; LHC, light-harvesting complex; LT, low temperature; MES, 2-(*N*-morpholino)ethanesulfonic acid; MGDG, monogalactosyldiacylglycerol; MOPS, 3-(*N*-morpholino)propanesulfonic acid; MPC, membrane protein complex; NFD, non-fat dry milk; OEC, oxygen-evolving complex; PAG, polyacrylamide gel; PAGE, polyacrylamide gel electrophoresis; PC, phosphatidylcholine; PG, phosphatidylglycerol; PI, phosphatidylinositol; PS, photosystem; pSMA, poly(styrene-co-maleic acid); pSMA-S, poly(styrene-co-maleic acid) salt; PVDF, polyvinylidene difluoride; RFU, relative fluorescence unit; SDGC, sucrose density gradient centrifugation; SDS, sodium dodecyl sulfate; SF, solubilized fraction; SMA, styrene-co-maleic acid; SMALP, styrene-co-maleic acid lipoparticle; SQDG, sulfoquinovosyldiacylglycerol; TBS, tris-buffered saline; TBS-T, tris-buffered saline – Tween-20; TEM, transmission electron microscopy; TEMED, *N,N,N',N'*-tetramethylethylenediamine; TM, thylakoid membrane; UV-vis, ultraviolet-visible.

* Corresponding author.

E-mail address: bbruce@utk.edu (B.D. Bruce).

¹ Present address: School of Molecular Sciences, Arizona State university, Tempe, AZ 85281.

<https://doi.org/10.1016/j.bbabio.2020.148347>

Received 10 July 2020; Received in revised form 9 November 2020; Accepted 21 November 2020

Available online 28 November 2020

0005-2728/© 2020 Elsevier B.V. All rights reserved.

extraction of native MPCs within nano-sized SMA lipoparticles (SMALPs). Knowing the relationship between polymer physicochemical properties and their solubilization efficacy can help in the design and synthesis of novel pSMA-S with tailored properties. However, despite the considerable progress in the understanding of how SMA polymers interact with many, well-studied membranes, there is still little work on the galactolipid-rich membranes found in thylakoids [13,17].

The highly dynamic nature of thylakoid membranes (TMs) [8,9], reflected both in vertical variability of grana stacking and in lateral heterogeneity [10], make them an interesting and challenging subject for study. These membrane properties suggest the existence of subdomains within the thylakoids which might be functionally specialized [11], enabling physically distinct TM regions for photosynthetic processes such as light harvesting, charge separation, proton pumping, cyclic electron transport, and ATP synthesis [12]. Previously [13], we tested the ability of twelve commercially available SMA copolymers with different physicochemical properties to extract MPCs from the most densely packed biological membrane – chloroplast TM. Fundamentally, the role of TMs in photosynthetic electron transport and energy conversion relies on close proximity of protein complexes, which results in a high protein-to-lipid ratio: 75% of membrane is occupied by protein complexes [1]. Additionally, TM lipid composition differs significantly from the composition of other subcellular compartments and biological membranes previously used in studies with pSMA-S. TMs are characterized by a low content (less than 20%) of phospholipids, mostly phosphatidylglycerol (PG), phosphatidylcholine (PC), and phosphatidylinositol (PI), and consist primarily of galactolipids: monogalactosyldiacylglycerol (MGDG), digalactosyldiacylglycerol (DGDG), and sulfoquinovosyldiacylglycerol (SQDG) [14,15]. The efficacy of membrane protein extraction by pSMAs from galactolipid-containing biomembrane can differ considerably [16] compared to phospholipid-containing membranes for which the application of SMA polymers have been mostly studied.

Based on the efficacy of both protein and chlorophyll extraction, we have found five SMA copolymers: SMA® 1440, XIRAN® 25010, XIRAN® 30010, SMA® 17352, and SMA® PRO 10235, that show promise in extracting supramolecular protein complexes from spinach TMs. The current study extends earlier works that demonstrated the application of SMA copolymers for solubilization of higher plant [13,17] and cyanobacterial [18] thylakoids. To advance the application of SMA copolymers for studying TM organization [17] we examined the correlation between physicochemical properties of five SMA copolymers and composition of isolated photosynthetic supramolecular protein complexes extracted from two biological membranes – spinach and pea TMs.

Appressed TMs enriched in photosystem II (PSII) were isolated from intact spinach and pea chloroplasts and subjected to one-step solubilization with five SMA copolymers. Extracted protein-containing SMALPs were resolved by sucrose density gradient centrifugation (SDGC) yielding high-density fractions (HDFs) of large supramolecular complexes. The composition of the HDFs were characterized by ultraviolet–visible (UV–Vis) spectroscopy, 77 K fluorescence emission spectroscopy, polyacrylamide gel electrophoresis (PAGE), and immunoblotting with 22 antibodies against subunits of major thylakoid multiprotein complexes: PSII and its light-harvesting complexes (LHCII), photosystem I (PSI) and cytochrome b_6/f complex (cyt. b_6/f). The new method of membrane protein isolation utilizing pSMAs may enable isolation of intact complexes and allow in vitro analysis of thylakoid heterogeneity to be studied more accurately. This extraction technique is also a timely complement to the progress made in advanced imaging methods such as cryo-electron tomography [19–21] and single particle, cryo-EM analysis [22–24], which have been applied to explore structure-function dynamics in these photosynthetic membranes [25].

2. Materials and methods

2.1. Materials

Amido black 10B (Bio-Rad, 161-0402); acetic acid (Fisher Chemical, A38-12); acetone (Fisher Scientific, A949); acetone for electron microscopy (Electron Microscopy Sciences, 10015); albumin standard (Pierce, 23209); ammonium persulfate (APS; Fisher BioReagent, BP179); L (+)-ascorbic acid, sodium salt (Fluka, BioChemica, 11140); bovine serum albumin (BSA) fraction V (United States Biochemical, 70195); Coomassie brilliant blue R-250 (CBB R-250; Fisher BioTech, BP101); *n*-dodecyl- β -D-maltoside (DDM) (GLYCON Biochemicals GmbH, D97002); dry milk (instant), non-fat (NFDM; Kroger); DL-dithiothreitol (DTT; Gold Biotechnology, Inc., DTT100); ethylenediaminetetraacetic acid (ICN Biomedicals, 101676); N,N,N',N'-ethylenediaminetetraacetic acid, tetrasodium salt, dihydrate (United States Biochemical, 15700); L-glutathione reduced (Sigma, G4251); glycerol (Fisher Bioreagent, BP229); glycine (Gold Biotechnology, G-630); HEPES (4-(2-hydroxyethyl)-1-piperazineethanesulfonic acid) (Fisher BioReagents, BP310); 1-hexadecane (TCI America, H061025ML); hydrochloric acid (Fisher Scientific, A142); lead citrate, trihydrate (Electron Microscopy Sciences, 17810); magnesium chloride, anhydrous (Acros Organics, 223210010); manganese chloride, tetrahydrate (Fisher Scientific, M-87); MES (2-(N-morpholino)ethanesulfonic acid) free acid monohydrate (Fisher BioReagents, BP300); methanol (Sigma-Aldrich, 179337); MOPS (3-(N-morpholino)propanesulfonic acid) (Gold Biotechnology, M-790); osmium tetroxide (Electron Microscopy Sciences; 19130); Percoll™ (GE Healthcare, 17-0891-09); polyoxyethylene-20-sorbitol monolaurate (Tween® 20; Fisher BioReagents, Fisher Chemicals, BP337); potassium chloride (Fisher Chemical, P217); potassium hydroxide (Fisher Scientific, P250); ProtoGel (30% acrylamide and 0.8% (w/v) N,N'-bisacrylamide stock solution, 37.5:1; National Diagnostic, EC-890); sodium carbonate, anhydrous (Fisher Scientific, BP 357); sodium dodecyl sulfate (SDS; Fisher Biotech, BP166); D-sorbitol (Fischer Scientific, S459); N,N,N',N'-tetramethylethylenediamine (TEMED; Fischer BioReagents, BP150); and tris base (Amresco, 0497); uranyl acetate (Electron Microscopy Sciences, NC0788109). All reagents were used as received without further purification. Distilled water additionally purified by Milli-Q® Q-Gard® 2 (Millipore Sigma) was used in experiments.

SMA copolymers utilized in this study and their physical properties are listed in Table I.

2.2. Methods

2.2.1. Hydrolysis of poly(styrene-co-maleic) acid anhydrides

For this study, commercially hydrolyzed SMA copolymers – poly(styrene-co-maleic acid) ammonium or sodium salts without additional purification were used. PRO 10235 supplied as anhydride was converted to ammonium salt by refluxing the polymer with continuous stirring in the presence of ammonium hydroxide at 75 °C for 5 h [13]. To avoid photooxidative degradation of copolymers due to photo-crosslinking

Table I
Physical properties of styrene-co-maleic acid polymers as specified by supplier.

Supplier	Product name	Styrene-to-maleic acid mole ratio	Mw [kDa]	Mn [kDa]	D (Mw/Mn)
Polyscope Polymers	XIRAN® SL 30010 S30	2:1	6.50	2.50	2.60
	XIRAN® SL 25010 S25	3:1	9.20	3.20	2.88
TOTAL Cray Valley	SMA® PRO 10235	1.5:1	7.00	2.90	2.41
	SMA® 1440H	1.7:1	7.00	2.80	2.50
	SMA® 17352H				

and chromophore formation [26], aqueous polymer solutions with mass fraction 10% were stored away from direct sunlight at room temperature.

2.2.2. Plant growth and isolation of crude thylakoid membranes from intact chloroplasts

Pea seeds (Progress #9, Jung Seeds) were imbibed overnight in cold water (~10 °C), planted on coarse (A-3) horticultural vermiculite (Palmetto Vermiculite Company) in autoclaved trays (35 cm × 50 cm), and grown in Environmental Growth Chamber (EGC TC-60) with a 12 h light cycle at 20 °C and 150 μmol m⁻² s⁻¹ photons from fluorescent (Philips, F72T12/CW/HO 85 W, 4100 K, 59 CRI & Sylvania 100 W) and incandescent (Westinghouse, 100 W, 2700 K) bulbs. Plants were watered every third day. Fifteen-day-old pea seedlings were harvested before the end of the dark cycle. Mature spinach leaves were purchased locally and stored overnight in the dark at 4 °C. Total TMs from intact chloroplasts were isolated from spinach leaves or pea seedlings according to a previously described method [13] adapted from Bruce et al. [27]. All preparative procedures were carried out on ice in dim lightning to minimize light-associated degradation of chlorophyll-containing proteins. This purification procedure yielded largely dark-adapted thylakoids.

2.2.3. Removal of stromal and peripherally associated proteins from crude thylakoid membranes

To remove stromal and peripherally associated proteins and facilitate membrane protein extraction, spinach and pea TMs were washed with 100 mM Na₂CO₃ according to a previously described procedure [13] adapted from Fujiki et al. [28]. Briefly, TMs were diluted threefold with 100 mM sodium carbonate solution and incubated on ice for 45–60 min. The suspension was then vortexed for a few seconds and centrifuged at 15,000g for 10 min at 4 °C. To completely remove sodium carbonate, the membrane pellet was washed subsequently with ice-cold GKB-150 (50 mM glycine-KOH buffer with pH 9.0, 150 mM KCl) and GKSB-150 (50 mM glycine-KOH buffer with pH 9.0, 150 mM KCl, 20% glycerol). The pellet, containing washed TMs, was finally resuspended in GKSB-150 at a final chlorophyll concentration of ~2 mg/mL, aliquoted, and stored at –20 °C until further use.

2.2.4. Solubilization of washed thylakoid membranes

TMs were solubilized by mixing equal volumes of washed TMs with protein concentration 3 mg/mL in GKSB-150 and pSMA-S solutions or *n*-dodecyl-β-D-maltoside (β-DDM) with mass fractions of 3.0 and 2%, respectively, in GKB-150, yielding final pSMA-S and DDM concentrations of 1.5 and 1.0%, respectively. The solubilization was carried out in the dark for 60 min at 40 °C with slight mixing on an orbital shaker (250 rpm). Non-solubilized TM fraction was then pelleted by centrifugation at 35,000g for 10 min at 4 °C. The supernatants containing the solubilized thylakoid membranes were carefully collected without disturbing the pellet and used for further analysis.

2.2.5. Separation and isolation of supramolecular membrane protein complexes

Supramolecular MPCs were separated by ultracentrifugation through a linear sucrose density gradient (0.2–1.2 M) in GKB-150 containing 0.01% solubilizing agent (pSMA-S or DDM) with or without a 2.0 M sucrose cushion. Gradients without a sucrose cushion were used to quantify the yield of chlorophyll-containing fractions, while gradients with a sucrose cushion were used for isolation, fractionation, and analysis of MPCs (Section 2.2.6).

The gradients were centrifugated at 100,000g for 20 h at 4 °C. Low-density fractions containing pigment-binding proteins and high-density fractions (HDFs) from sucrose density gradients with a sucrose cushion were collected using a syringe. Pellets, HDFs, from sucrose density gradients without a sucrose cushion were resuspended in a minimal volume of resuspending buffer (GKRB-150: 50 mM glycine-KOH buffer with pH 9.0, 150 mM KCl, 10% glycerol). To further resolve the

pigment-binding protein complexes from HDFs, the fractions collected with a syringe were overlaid onto second linear sucrose density gradients (1.2–2.0 M) and centrifugated again.

Samples containing solubilized TM fractions and supramolecular protein complexes from HDFs were further analyzed by UV-Vis spectroscopy (Section 2.2.8), low temperature (LT) fluorescence emission spectroscopy (Section 2.2.9), SDS-PAGE (Section 2.2.12), and immunoblotting (Section 2.2.13). The total protein content was determined using bicinchoninic acid (BCA) assay or densitometric analysis of Coomassie stained polyacrylamide gels (PAGs) (Section 2.2.10), while total chlorophyll, chlorophyll *a*, and chlorophyll *b* was quantified after its extraction with 80% aqueous acetone solution (Section 2.2.11). Solubilization efficacy (Section 2.2.14) was calculated according to a previously described method [13].

2.2.6. Fractionation and analysis of supramolecular membrane protein complexes

Supramolecular MPCs, after being separated by sucrose density gradient centrifugation (SDGC) (Section 2.2.5), were additionally fractionated and analyzed using the density gradient fractionator (ISCO, model 185) which consists of the tube holder with an attached on the top UV absorbance flow cell, a pump, and an absorbance/fluorescence monitor (ISCO UA-5). Absorbance was measured at 254 nm with a flow rate of 0.75 mL/min. Data points were extracted using the DATA acquisition software (DATAQ instruments).

2.2.7. Transmission electron microscopy and chloroplast structure analysis

Isolated intact chloroplasts from pea seedlings and spinach leaves were prepared for transmission electron microscopy (TEM) via high-pressure freezing and quick freeze-substitution [29]. Briefly, an intact chloroplast pellet was mounted in an aluminum specimen holder with 1-hexadecene as a cryoprotectant. Samples were frozen with a Wohlwend Compact 02 high-pressure freezer (Technotrade International, Inc.) and placed into fixation tubes with 1% osmium tetroxide and 0.1% uranyl acetate in acetone and stored in liquid nitrogen. Quick freeze-substitution was performed according to the previously described method [29]. Once at room temperature, samples were washed with 100% acetone and embedded in Embed 812 epoxy resin (Electron Microscopy Sciences, 14,120). Blocks were thin-sectioned and sections were mounted on copper mesh grids (Ted Pella, Inc., 1GC400). Mounted sections were stained with Reynold's lead citrate and imaged with a JEOL 1400 Flash transmission electron microscope operating at 80 kV. Number of grana per chloroplast section, grana height, and the number of layers per granum were determined for both spinach and pea samples using Fiji, an open-source image processing package based on ImageJ [30].

2.2.8. UV-vis spectroscopy

UV-vis spectra of samples, diluted with GKRB-150 to 2–20 μg/mL of total chlorophyll, were recorded between 200 and 800 nm (1 nm bandwidth, 240 nm/min) in a quartz cuvette with a pathlength of 1 cm using double/split beam UV-vis spectrophotometer Evolution 300 (Thermo Scientific). All spectra were background corrected.

2.2.9. LT fluorescence emission spectroscopy

Fluorescence emission spectra of samples diluted with GKRB-150 to 4–5 μg/mL of total chlorophyll were recorded within 600–800 nm wavelength range (3 nm slit width, 1 nm step, 0.5 s integration time) at 77 K (–196 °C) using a Photon Technology International Quanta Master fluorometer (Horiba Scientific). The samples were excited at 435 nm. Three spectra were averaged for each measurement, background corrected, and deconvoluted with three Gaussian functions in OriginPro 2018. The maximum for the three peaks at approx. 680, 695, and 725 nm and the area ratio of peak 3 to peak 2 were calculated.

2.2.10. Protein quantification

BCA protein colorimetric assay (Pierce BCA Protein Assay Kit, 23227) was used to quantify the total protein content in samples according to the manufacturer's microplate protocol. Absorbance at 540 nm was measured at 25 °C using a LabSystem Multiscan MCC/340 (Fisher Scientific) microplate reader. The average absorbance of a blank solution was subtracted from the average absorbance of individual standards and samples. The BSA calibration curve (0–2 mg/mL), fitted to a quadratic function ($A_{norm} = aC^2 + bC$), was used to estimate the total protein concentration in samples. The protein concentration in HDF-SMALPs was quantified densitometrically in Coomassie stained polyacrylamide gels (12% RunBlue™ bis-tris protein gels [Expdeon, NBT01227] run with MOPS buffer [Expdeon, NXB75500]). Total protein concentration was estimated using BSA calibration curve (0.1–2.5 µg per well) fitted to a linear function ($I_s = aC + b$). The signal intensity (I_s) was measured in Image Studio Lite (LI-COR Biosciences, version 5.2). The protein yield was normalized to untreated TM control.

2.2.11. Chlorophyll quantification

Chlorophyll *a* and *b* were extracted from the samples (25 µL) with 80% aqueous acetone solution (975 µL) according to a previously described method [13], and quantified using equations derived by Porra et al. [31]. The chlorophyll yield was normalized to untreated TM control.

2.2.12. Electrophoresis

The polypeptide profile of samples using discontinuous glycine-sodium dodecyl sulfate-polyacrylamide gel electrophoresis (SDS-PAGE) [32] with 15% resolving gel, tricine-SDS-PAGE [33] with 12% resolving gel, or precast 12% RunBlue bis-tris protein gels run with MES buffer (Expdeon, NXB70500) or MOPS buffer. RunBlue lithium dodecyl sulfate (LDS) sample buffer (Expdeon, NXB32010) and RunBlue DTT reducer (Expdeon, NXA32001) were used to prepare reduced samples for protein electrophoresis. All samples were denatured by heating for 15 min at 65 °C. Electrophoresis was carried out at constant voltage of 75 V and 150 V for stacking and resolving gels, respectively, for glycine/tricine-SDS-PAGs or by running precast gels at 175 V. Mark 12 unstained (Invitrogen, LC5677) or Precision Plus Protein all blue prestained (Bio-Rad, 1610373) protein standards were used to estimate polypeptide apparent size in ImageLab 6.0.1 (Bio-Rad). Proteins were visualized directly in the gel by staining with CBB R-250 [13], InstantBlue Protein Stain (Expdeon, ISB1L), or transferred onto polyvinylidene difluoride (PVDF) membrane and further immunodetected with specific antibodies (Section 2.2.13). Gels were imaged using ChemiDoc MP imaging system (Bio-Rad, 12003154).

2.2.13. Immunoblot analysis

Twenty-two specific antibodies (listed in Table II) against subunits of major thylakoid MPCs were tested. Polypeptides separated by gel electrophoresis were subsequently electrotransferred for 30 mins at 25 V onto 0.45 µm Immobilon-FL (Millipore Sigma, IPFL00010) or 0.20 µm PVDF membrane (Invitrogen, LC 2002) using trans-blot turbo transfer system (Bio-Rad) and Towbin transfer buffer (TB) [34] containing 25 mM Tris base, 192 mM glycine, 20% methanol with 0.01% SDS, pH 8.3. Standard immunodetection procedure was used for protein identification. Tris-buffered saline containing 0.1% Tween-20 (TBS-T) was used for washing, while TBS-T with 5% non-fat dry milk (TBST-T-NFDM) – for blocking and incubation with primary and secondary antibodies.

Proteins of interest were detected using fluorophore-conjugated secondary antibodies (StarBright Blue 520 goat anti-rabbit IgG, Bio-Rad, #12005870; Alexa Fluor Plus 555 goat anti-chicken IgY, Invitrogen, #A32932; Alexa Fluor Plus 488 goat anti-rabbit, Invitrogen, #A32731), or goat anti-rabbit horseradish peroxidase-conjugated secondary antibodies (Jackson ImmunoResearch Laboratories, # 111-035-144) detected using the SuperSignal™ West Dura Extended Duration Chemiluminescent Substrate (Thermo Scientific, #34076) was used as a

Table II

Information on primary antibodies: company name, product number, and dilution used.

Membrane protein complex	Primary antibody	Company	Product number	Dilution	
LhcII	<i>α</i> -Lhcb1	Agrisera	AS01 004	1 : 2000	
	<i>α</i> -Lhcb1	PhytoAB	PHY0487S	1 : 1000	
	<i>α</i> -Lhcb2	PhytoAB	PHY0086S	1 : 5000	
	<i>α</i> -Lhcb3	PhytoAB	PHY0087S	1 : 1000	
	<i>α</i> -Lhcb4	PhytoAB	PHY0044A	1 : 5000	
	<i>α</i> -Lhcb5	PhytoAB	PHY0667S	1 : 10,000	
	<i>α</i> -Lhcb5	PhytoAB	PHY0088S	1 : 5000	
	<i>α</i> -Lhcb6	PhytoAB	PHY0089S	1 : 1000	
	PSII	<i>α</i> -PsbA	PhytoAB	PHY0103	1 : 1000
		<i>α</i> -PsbB	Agrisera	AS04 038	1 : 1000
		<i>α</i> -PsbO	PhytoAB	PHY0344	1 : 5000
		<i>α</i> -PsbO	PhytoAB	PHY0094A	1 : 1000
<i>α</i> -PsbP		PhytoAB	PHY0061S	1 : 1000	
<i>α</i> -PsbP		PhytoAB	PHY0646S	1 : 1000	
<i>α</i> -PsbQ		PhytoAB	PHY0081S	1 : 1000	
<i>α</i> -PsbR		PhytoAB	PHY01100A	1 : 1000	
<i>α</i> -PsbW		PhytoAB	PHY01110A	1 : 1000	
PSI		<i>α</i> -PsaD	BDB lab	n/a	1 : 15,000
	<i>α</i> -PsaF	BDB lab	n/a	1 : 1000	
Cytochrome <i>b</i> ₆ / <i>f</i>	<i>α</i> -subunit IV	BDB lab	n/a	1 : 5000	
	<i>α</i> -cytochrome <i>b</i> ₆	BDB lab	n/a	1 : 5000	
	<i>α</i> -cytochrome <i>f</i>	BDB lab	n/a	1 : 15,000	

Note: the antibody highlighted with gray did not cross-react with both spinach and pea TMs under the studied conditions.

chemiluminescent substrate. After proteins of interest were immunodetected and imaged, all proteins were visualized by staining with amido black [34]. Blots were imaged using ChemiDoc MP imaging system and analyzed in ImageLab 6.0.1. Image studio Lite 5.2 was used for quantification of fluorescent and chemiluminescent signals.

2.2.14. Solubilization efficacy

Solubilization efficacy [%] of pSMA-S and DDM was estimated as a ratio of total protein or total chlorophyll in solubilized TM fraction to the concentration of proteins or chlorophylls in the sample before centrifugation [13].

2.2.15. Statistical analysis

The data are presented as an arithmetic mean ± confidence interval for 1 σ (~68%) [13,35]. The representative experiments have been shown in the paper. The experiments on chlorophyll and protein quantification have been repeated ~40 times using TMs from at least 3 different preparations. The experiments including sucrose gradient ultracentrifugation and chlorophyll fluorescence emission and UV-vis spectroscopy have been repeated at least 3 times, while the analysis and fractionation was carried out *t* times using the same TM preparations. Western blot experiments were repeated at least twice for each antibody; different TM preparations were used. One-way analysis of variance (ANOVA) with Dunn-Sidak comparison test or two-tailed *t*-test were used for significance testing with a significance level of $\alpha = 0.05$. Mann-Whitney *U* tests for nonparametric data were performed in GraphPad Prism (GraphPad Software, Inc.). All other calculations were performed using Microsoft Excel (Microsoft), while OriginPro 2018 (OriginLab Corporation, version b9.5.0.193) were for plotting graphs, analyzing and deconvoluting peaks, nonlinear and linear fitting, statistical analysis, and graphical residual analysis. MarvinSketch 2017 (ChemAxon, version 17.4.3) was used for drawing and displaying chemical structures.

3. Results and discussion

3.1. Extraction efficacy

The main challenge of sample preparation for structural and functional analysis of membrane proteins is establishing experimental conditions under which the protein complex of interest can be isolated from biological membranes in its native conformation and lipid environment. In previous studies [1,36], it was shown that subtle changes of detergent properties could alter their towards thylakoids, when it was reported that two isomeric forms (α - and β -) of the traditional detergent *n*-dodecyl-D-maltoside (DDM) have different solubilizing effects on TMs. However, to date there has not been a report on how chemical modifications of the SMA copolymers can alter solubilization of lipids [37] or membrane proteins [38]. To study the solubilizing effect of copolymers during extraction of thylakoid supramolecular MPCs we utilized five SMA polymer derivatives: three unmodified poly(styrene-*co*-maleic acid) salts (pSMA-S) (PRO 10235 and 30010 and 25010) and two esters (1440 and 17352). The schematic structures of polymers are shown in Fig. 1. The polymer physical properties can be found in Table I.

Spinach and pea TMs were solubilized in a single step with 1% β -DDM (positive control) or 1.5% pSMA-S (Section 2.2.4). To facilitate the membrane protein extraction from densely packed thylakoids, the solubilization was carried out at 40 °C for an hour with mixing. Unsolubilized TM was separated from solubilized fraction (SF) by high-speed centrifugation (35,000 g) and the solubilization efficacy was estimated (Section 2.2.14). The solubilization efficacy of SMA polymers depends not only on the physicochemical properties of the polymers but it is also defined by the intrinsic properties of the starting thylakoids (Fig. 2). As we have observed previously [13,18], SMA polymer 1440 has the highest extraction yield for TMs from both chloroplasts and cyanobacteria, yet with SMA 1440 solubilization yields are always below the DDM recovery. Interestingly, the SMA1440 which is the highest performing SMA is a modified form of PRO 10235, which is the lowest performing SMA based on protein and chlorophyll extraction in both spinach and pea thylakoids. This suggests that the functional group, butoxyethanol, increases this polymers interaction with thylakoid membranes and/or ability to solubilize chlorophyll-containing membrane proteins.

3.2. Thylakoid structural morphology differences between spinach and pea chloroplasts

Interestingly, we observed higher extraction yield of both proteins (32.6 (\pm 12.4) % on average) and chlorophylls (61.7 (\pm 6.7) % on average) from pea chloroplasts then from spinach chloroplasts (Fig. 2B

and C, respectively). The increase in protein-to-chlorophyll and chlorophyll *a/b* ratio indicates the enrichment of a particular membrane protein complexes. These results could be due to differences in growth conditions such as temperature and illumination level, or the maturity and greening state of the plant, or both. In addition, fundamental differences in membrane lipid composition and protein-to-lipid ratio can also affect solubilization efficacy. To help clarify the differences in the starting thylakoids, we studied the structure of isolated intact chloroplasts using TEM (Fig. 3). The results of microscopy indicate clear differences in the thylakoid organization in these two types of chloroplasts. The size and number of stacks in the grana are much larger in the spinach chloroplast (Fig. 3A) compared to the pea chloroplasts (Fig. 3B).

Morphometric analysis of hundreds of chloroplasts from both organisms revealed that although spinach chloroplasts did not have significantly more grana than pea chloroplasts (\sim 30 per cross-section, Fig. 3C, $p = 0.2633$), on average the grana of spinach had more stacks than pea (\sim 12 vs. 7, Fig. 3D, $p < 0.0001$) and the thickness of the spinach grana were significantly higher (250 nm vs. 150 nm, $p < 0.0001$). This analysis confirms the visual observation that pea chloroplasts have more stromal lamellae than grana lamellae, resulting in a much higher thylakoid surface area per unit protein or chlorophyll as compared to the spinach grana with higher protein density. This may be one of the reasons for the difference in the higher yield of pea complex extraction.

Although it is evident that the two chloroplasts have different ultrastructure, the reasons for this are unclear. One possibility can be related to the plant growth conditions, for example, the spinach plants were field grown and would have been exposed to the much higher light intensities (\sim 1500 $\mu\text{mol m}^{-2} \text{s}^{-1}$) than the light conditions used to grow pea seedlings (150 $\mu\text{mol m}^{-2} \text{s}^{-1}$). In addition, the spinach leaves were from mature plants while the peas were harvested from 15-day old seedlings. It is possible, that advanced leaf maturation and the higher light intensity contributed to the increase stacking of the spinach grana and an overall decrease in the solubilization efficacy.

Banerjee et al. [44] demonstrated that the intactness of solubilized MPCs depends on the coextraction of lipids with the protein complex. Thus, it is also possible that the difference in the solubilization efficacy between two types of TMs may be explained by species-specific differences in the lipid and fatty acid composition (Table SI) and/or protein-to-lipid ratio which can be affected by difference in growth conditions.

Membrane properties such as fluidity, thickness, lateral pressure, and charge density all contribute to the protein extraction by SMA polymers [37]. Although the lipid class composition of spinach and pea TMs is similar (Table SII), in spinach an 18C:16C lipid ratio of fatty acids is 4.4 ± 0.9 , reflecting the fact that spinach is a 16:3 plant. However, in pea, which is an 18:3 plant, this ratio is much higher, approaching 14.8

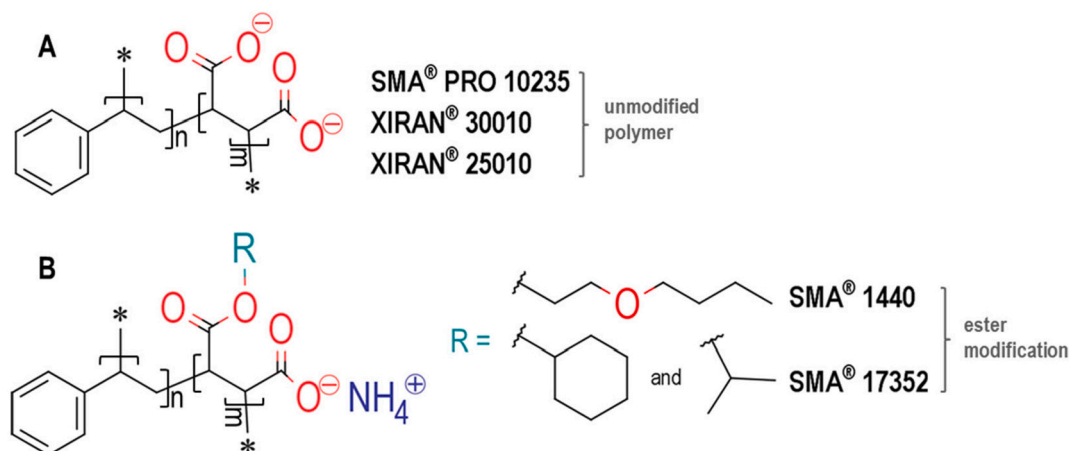


Fig. 1. Chemical structure of polymer solubilizing agents: derivatives of poly(styrene-*co*-maleic acid) – unmodified polymer salt (A) and ester modification (B). Note: n and m stand for number of styrene and maleic acid units.

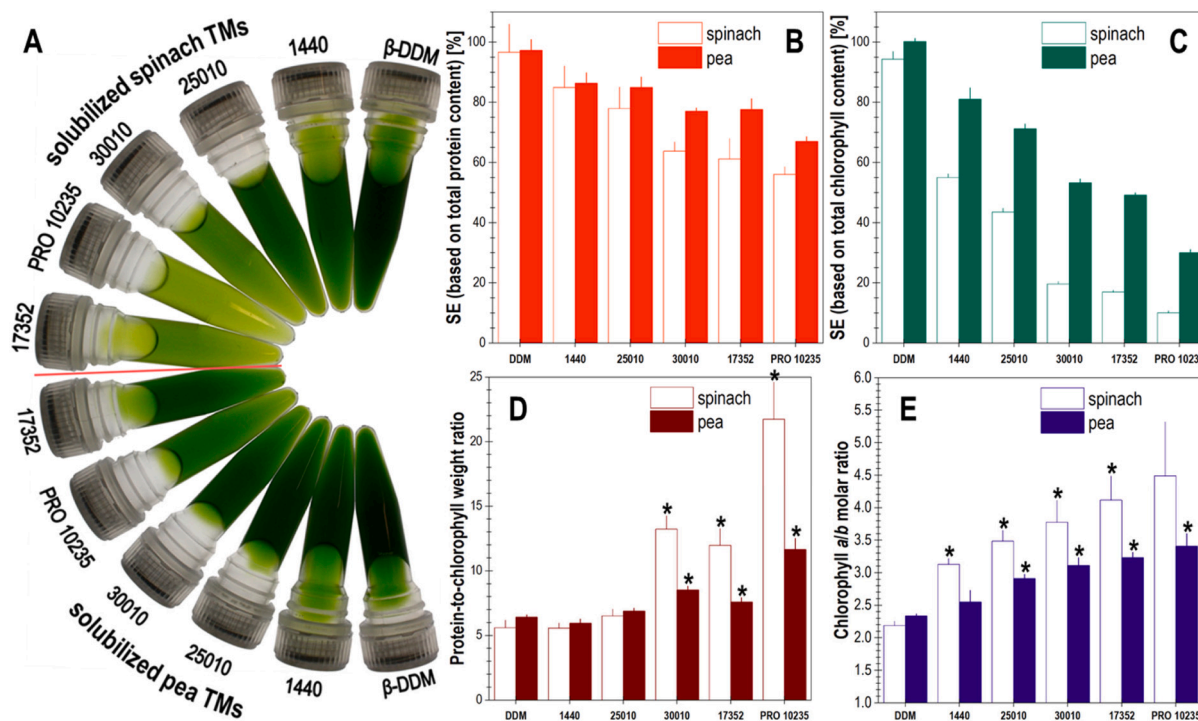


Fig. 2. Characterization of TMs solubilized with SMA polymers. Photo of solubilized spinach and pea thylakoid membranes (A) and protein and chlorophyll quantification (B-E): solubilization efficacy estimated based on total protein content (B) or total chlorophyll content (C); protein-to-chlorophyll mass ratio (D); and chlorophyll a/b mole ratio (E). Samples in D and E whose means significantly differ from the control DDM sample at the 0.05 level are marked with an asterisk.

± 3.0 . In both species, all lipids are predominantly unsaturated. Based on previously published data [39] we estimated the unsaturation degree or index of hydrogen deficiency (IHD). For both species, spinach and pea TMs, IHD was 2.7 ± 0.3 . Despite the difference in growth temperature, only a slight difference in fatty acid unsaturation degree is expected for the plants [40]. Chapman et al. [40] also showed that the most clear change in TM composition due to temperature difference was in the protein-to-lipid mass ratio, which was higher in the warm-grown pea plant TMs for which the ratio was equal to 1.724. This difference may be important since the protein-to-lipid ratio could be one of the main factors which contributes to the regulation of membrane fluidity. Thus, higher solubilization efficacy of pea TMs compared to spinach TMs could also be explained by increased membrane fluidity and lateral pressure due to the presence of higher amount of longer (18:3) unsaturated fatty acids in addition to the lower protein-to-lipid ratio. Future work will help to clarify the differences in how SMA copolymers interact with thylakoid membranes.

Besides differences in solubilization efficacies, the protein-to-chlorophyll and chlorophyll a/b ratios (Fig. 2D and E) also differ significantly for TMs solubilized with polymers when compared to the positive control – β -DDM (for *p*-values refer to Table SIII). This could be due to the differential extraction of membrane proteins by SMA copolymers and is further addressed in Section 3.3.

3.3. Analysis of extracted thylakoid membrane protein complexes

Supramolecular protein complexes from spinach and pea solubilized TM fractions were further separated using 0.2–1.2 M sucrose density gradient centrifugation (Section 2.2.5), analyzed (Fig. S2), and fractionated. The samples were loaded onto the gradients with a sucrose cushion based on equal total chlorophyll content (Fig. 4) or without a sucrose cushion based on equal volumes (Fig. S1).

Fig. 4A and C illustrate the sucrose density profiles of separated spinach and pea pigment-containing protein complexes from TMs solubilized with β -DDM and SMA copolymers. Low-density bands (red

dots) were more diffuse and only partially resolved, suggesting either heterogeneity or variations in assembly of extracted membrane protein complexes (Fig. 4). High-density bands (purple squares) were observed for TMs solubilized with SMA (Fig. 4A and C). Due to the increased interest in isolation of intact PSII-LHCII complex for biochemical and structural studies [36], we further tried to resolve the supramolecular protein complexes, which we denoted as HDF-SMALPs, using a second 1.2–2.0 M SGDC (Fig. 4B and D).

Solubilization of TMs yields HDF-SMALPs between 10% and 35% based on starting chlorophyll (Fig. S3). In the case of spinach TMs, SMA polymers 25010 and 30010 are the most efficient in extraction of pigment-containing supramolecular MPCs, and PRO 10235 is the least efficient. For pea TMs, the efficacy in extraction of supramolecular protein complexes in the following series: PRO 10235 \approx 30010 \approx 25010 $>$ 17352 $>$ 1440.

From Fig. 4A and C, it can be concluded that SMA polymers 30010 and PRO 10235 extract supramolecular protein complexes with smaller sizes and/or lower density. To assess the heterogeneity of HDF-SMALPs, they were further separated on 1.2–2.0 M linear sucrose density gradients. Fig. 4B and D reveal that some HDF-SMALPs consist of at least two discrete pigment-containing particle populations. The number of populations in HDF-SMALPs is defined by the polymer type and the intrinsic properties of the starting thylakoids. No correlations have found neither with styrene-to-maleic acid ratio (s/ma) nor polymer molecular weight. Based on the number and heterogeneity of distinct bands in HDF-SMALPs, we classified the polymers into two distinct groups. The first group contains two unmodified polymers (30010 and PRO 10235) which yield one or two low density bands for HDF-SMALPs, while the second group contains three pSMAs (two esters, 1440 and 17352, and one non-ester polymer 25010). The polymers from the latter group extract a larger and/or denser MPC in addition to the diffuse band containing smaller and/or less dense MPCs. Given that previously we have not been able to find the correlation between physical properties and solubilization efficacy [13], these differences may be explained by the differences in polymer surface-active properties, which depends on

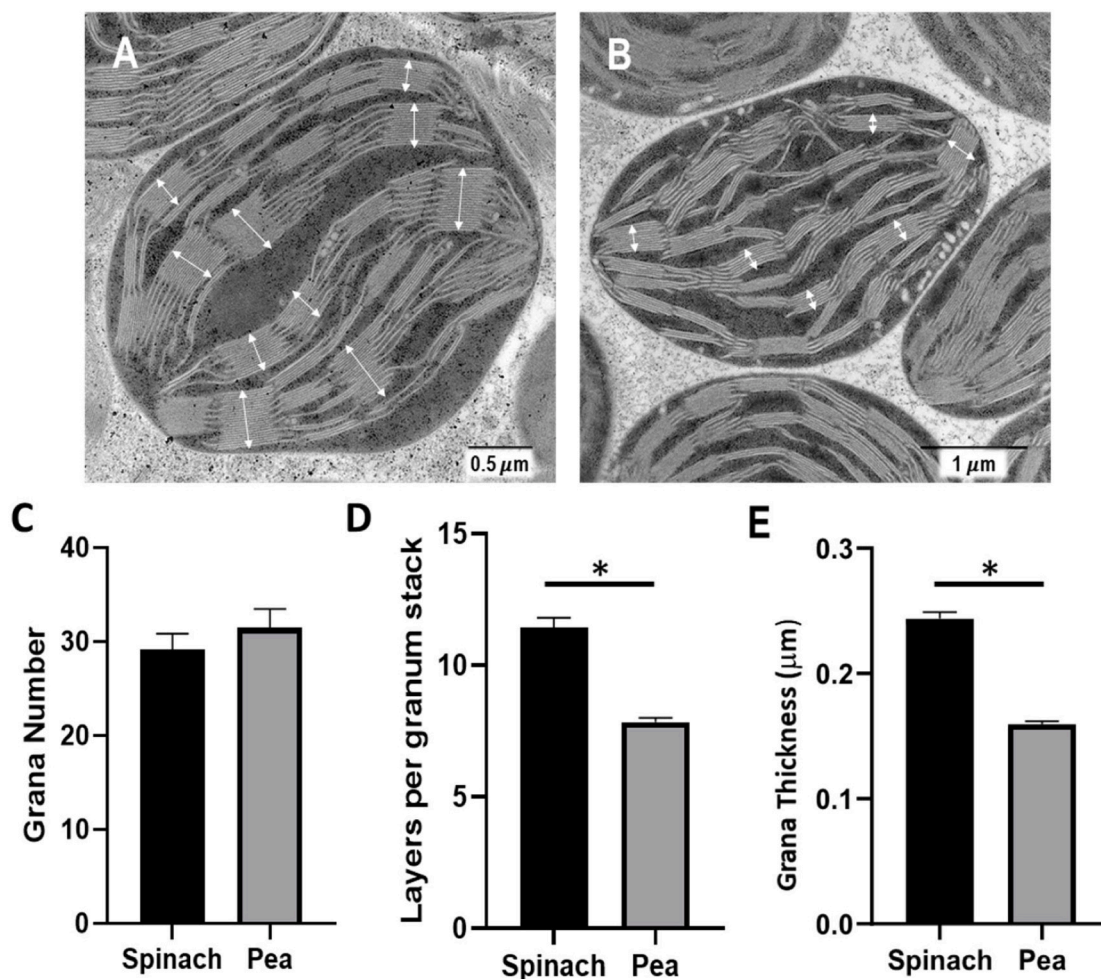


Fig. 3. Analysis of chloroplast morphology by TEM: representative electron micrograph of intact spinach (A) and pea (B) chloroplasts; grana number per chloroplast section ($N = 39$ (spinach) and 33 (pea); C), number of layers per granum ($N = 574$ (spinach) and 573 (pea); D), and grana thickness ($N = 1105$ (spinach) and 1038 (pea); E). Scale bar is 500 nm (A) and 1 μm (B). Asterisks denote statistical significance according to Mann-Whitney U test ($p < 0.05$).

polymer chemical composition and structure. The difference in surface-active properties can result in different polymer-lipid and polymer-protein interactions with TMs and yield distinct SMALPs with different sedimentation properties.

SMA copolymers contain two chromophore groups: a carbonyl group and a benzene ring which absorb at 180 nm ($\epsilon = 65,000$), 200 nm ($\epsilon = 8000$), and 254 nm ($\epsilon = 240$). To identify the free polymer and non-pigment-containing SMALPs we analyzed the absorption profiles of sucrose density gradients (Fig. S2). The SMA copolymer distribution was determined from absorption profiles of sucrose density gradients measured at 254 nm (Fig. S2). Free SMA polymer and low-density SMALPs were observed at the top of sucrose density gradients as overlapping peaks. The high-density SMALPs were located towards the bottom (Fig. 4). Additionally, we observed a few discrete populations of non-pigment containing supramolecular complexes eluted between 600 and 700 s for solubilized thylakoid membranes with 1440 , 25010 , 30010 , and 17352 polymers.

The pigment composition of both SFs and HDF-SMALPs was analyzed using UV-vis spectroscopy (Section 2.2.8). The light harvesting capabilities of the reaction centers in higher plants is extended by membrane-embedded light-harvesting systems that contain both chl a and b . These pigments are associated with membrane-bound antenna complexes known as light-harvesting complexes (LHCs) [41]. In higher plants, two distinct classes of LHCs can be distinguished: four LHCs which are exclusively associated with PSI (Lhca1–4) [41,42], and six LHCs – associated preferably (Lhcb1 and Lhcb2) or exclusively with PSII

(Lhcb3–6) [41,43]. Interestingly, although the chl a/b ratios are quite similar for DDM extracts of pea and spinach thylakoids (ratio ~ 2.5), extraction using the different pSMAs is species-specific and yields MPCs with higher chl a/b ratio compared to DDM control (Fig. 2E). The highest chl a/b ratio was observed for both spinach and pea thylakoid MPCs extracted with PRO 10235. When we carefully investigated the spectra of MPCs (unfractionated and HDF-SMALPs), we also found considerable variations in the content of carotenoids and other UV absorbing molecules (300 – 350 nm range). From a comparison of the absorbance spectra of solubilized spinach and pea TM fractions (Fig. 5A and B), one can see that SMA polymers have a similar trend in extracting pigment-containing complexes from two types of plant TMs. Notably, the relative content of chl a , chl b , and different types of carotenoids depends on the nature of the solubilizing agent. Comparing the absorption spectra around 650 nm, it is evident that the complexes isolated with PRO 10235 contain the least amount of chl b resulting in the highest chl a/b mole ratio, which is in accordance with determined chl a/b ratios (Figs. 2 and S4). The clear increase in chl a/b ratio in SFs and HDF-SMALPs may reflect an increased content of PSI and/or PSII. Alternatively, it may reflect the selective removal of the Chl b -containing LHC complexes. The carotenoid content (maximum around 470 nm) is the highest for DDM fraction followed by the 1440 fractions and it is the lowest for PRO 10235 fractions, with three other polymers in between. This observation supports a reduction in LHC content in these fractions.

To examine the association of LHCII trimers with PSI and PSII complexes for SFs and HDF-SMALPs, we studied low temperature

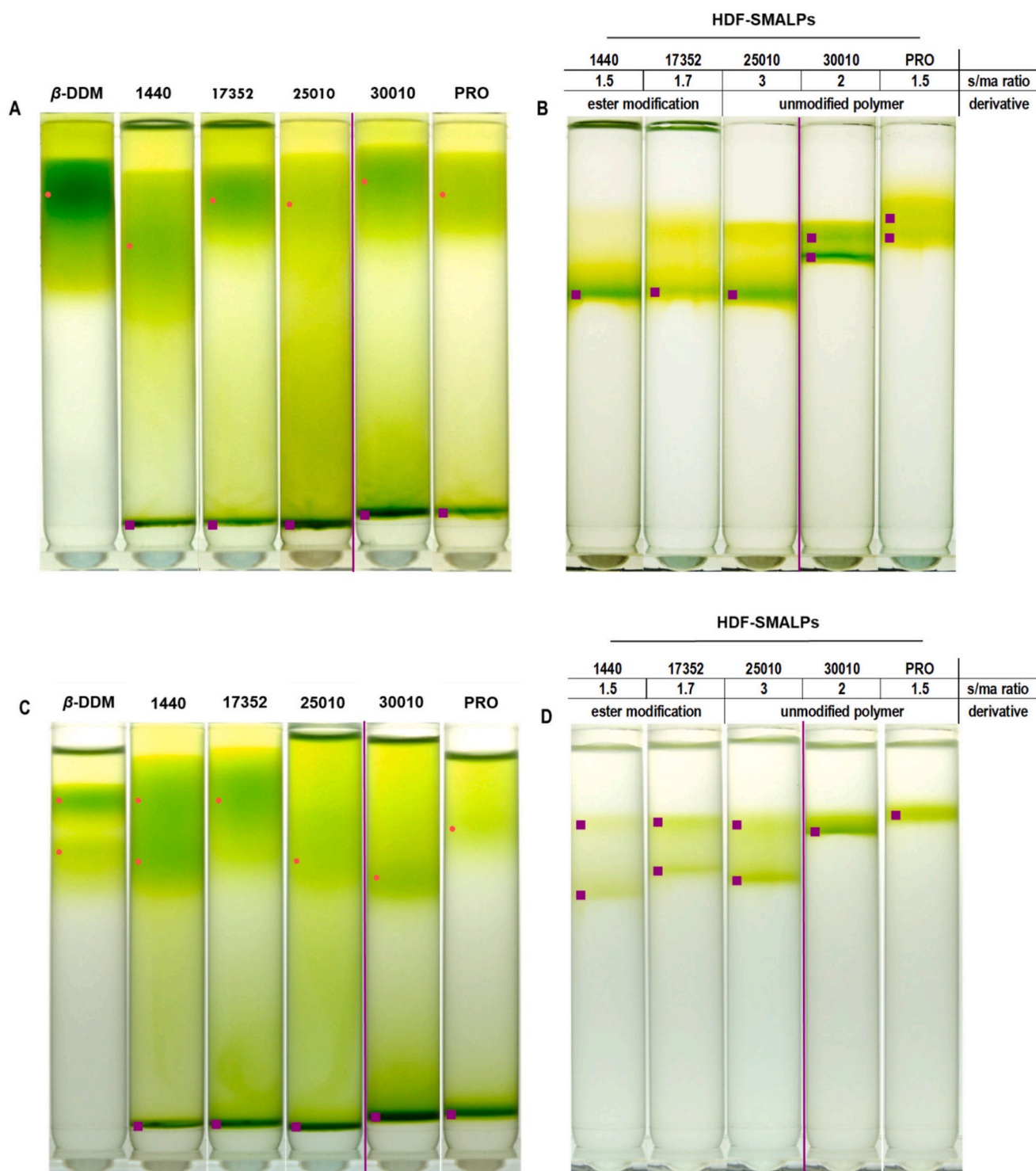


Fig. 4. Separation of supramolecular membrane protein complexes isolated from spinach and pea thylakoid membranes by sucrose density gradient ultracentrifugation: photos of solubilized spinach (A) and pea (C) pigment-binding protein complexes separated on 0.2–1.2 M linear sucrose density gradient with 2.0 M cushion; photos of spinach (B) and pea (D) high-density fraction (HDF, indicated by purple squares in A and C) after separation on 1.2–2.0 M linear sucrose density gradient. Gradient volume is 10 mL; sample loading – 150 μ g of total chlorophyll for A (\dagger 75 μ g for PRO 10235 fraction) and D and 25 μ g for B (\dagger 20 μ g for PRO 10235 fraction) and C. Red dots indicate pigment-containing protein bands. Note: s/ma stands for styrene-to-maleic ratio.

fluorescence emission (Fig. 6). To avoid artifacts during spectra collection (due to scattering and self-absorption/quenching, which lead to relative decrease in fluorescence yield of the bands associated with PSII (685 and 695 nm) and the red shift of fluorescence emission spectra), a dilution series were used to find an optimal sample concentration (Fig. S5). The SFs have a fluorescence emission maximum around 680

nm, characteristic of free chlorophyll and LHCII, with pronounced shoulders on both sides, while HDF-SMALPs are characterized by the presence of three maxima: around 680, 695, and 725 nm which can be assigned to CP47/CP43, CP47/PSII core complex, and PSI core complex, respectively [44]. In plants, chlorophyll associated with the PSII reaction center fluoresce at 685 and 695 nm – due to the main transition

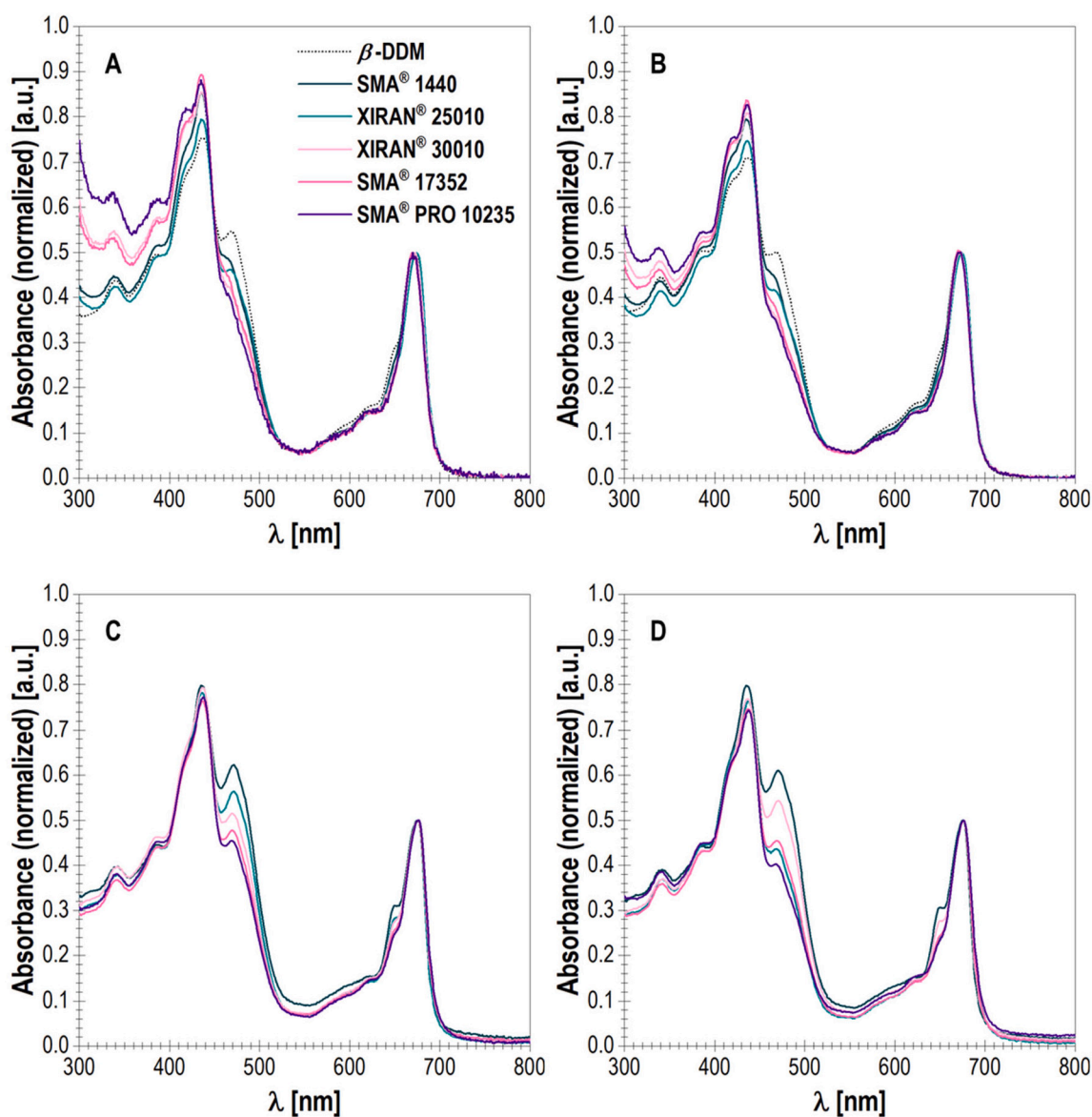


Fig. 5. Absorption spectra: UV-vis spectra of solubilized spinach (A) and pea (B) thylakoid membranes and spinach (C) and pea (D) HDF-SMALPs. The spectra are normalized to the maximum in the red region. Solubilized and high-density fractions were diluted 25 and 2 times, respectively, in GKRB-150, pH 9.0.

emission, and around 725 nm – due to self-absorption enhanced fluorescence in this region [44]. The absence of the 680 nm fluorescence emission peak confirms that the HDF-SMALPs do not contain free chlorophyll and moreover, the low relative fluorescence at 695 nm suggest that the SMA isolation largely preserves the supramolecular organization with the peripheral antennae chlorophyll remaining efficiently coupled to the PSI/PSII reaction centers. Fluorescence emission from chlorophylls within the PSI reaction center is emitted as a single broad band centered around 725 nm. These two peaks can be observed in solubilized TM fractions (Fig. 6A and B), indicating the presence of both intact and partially disassembled PSI- and PSII-containing complexes. To estimate the ratio between PSI and PSII/LHCII in HDF-SMALPs, the fluorescence spectra was deconvoluted (Fig. S6), and peak maximum and the area ratio of peaks centered at ~696 and ~720 nm for spinach or ~697 and 722 nm for pea were determined (Table III). The data suggest that the ratio of PSI-to-PSII/LHCII in the HDFs is variable for both spinach and pea isolations, and, depending on the type of SMA copolymer, it decreases in the following order: PRO 10235 > 30010 > 17352 > 25010 > 1440. Although peak integrations are only proportional and not absolute indicators, the variability in this ratio

would suggest that the different SMA polymers may yield different supramolecular complexes, they do follow a similar trend with the peak area ratios (A725/A695) that vary from 0.8 to 10.2 for spinach and from 1.7 to 95.7 for pea samples.

The polypeptide profile for spinach and pea solubilized fractions (Fig. S7) indicates the differential solubilization of MPCs as local changes in polypeptide profile. The overall purity and polypeptide composition of HDF-SMALPs was assessed by gel electrophoresis under equal chlorophyll loading (0.2 µg per well). The polypeptide profiles of HDF-SMALPs and TMs are shown in Fig. S8. HDF-SMALPs are highly depleted of proteins in 30–50 kDa molecular weight region, exhibiting major bands around 55 kDa, 20–30 kDa region, and a few bands around 15 kDa (Fig. S8).

To further examine the composition of HDF-SMALPs we performed immunoblot analysis with antibodies against subunits of major thylakoid MPCs: photosystem II and light-harvesting complex II, photosystem I, and cytochrome *b₆/f*. Fig. 7 and Table SIV & V show that HDF-SMALPs are highly depleted of PsbO, PsbP, PsbQ (pea), cyt. *b₆*, cyt. *f*, subunit IV, and PsfA indicating that they do not have detectable amount of oxygen-evolving complex (OEC) of PSII and cytochrome *b₆/f*. The antibodies

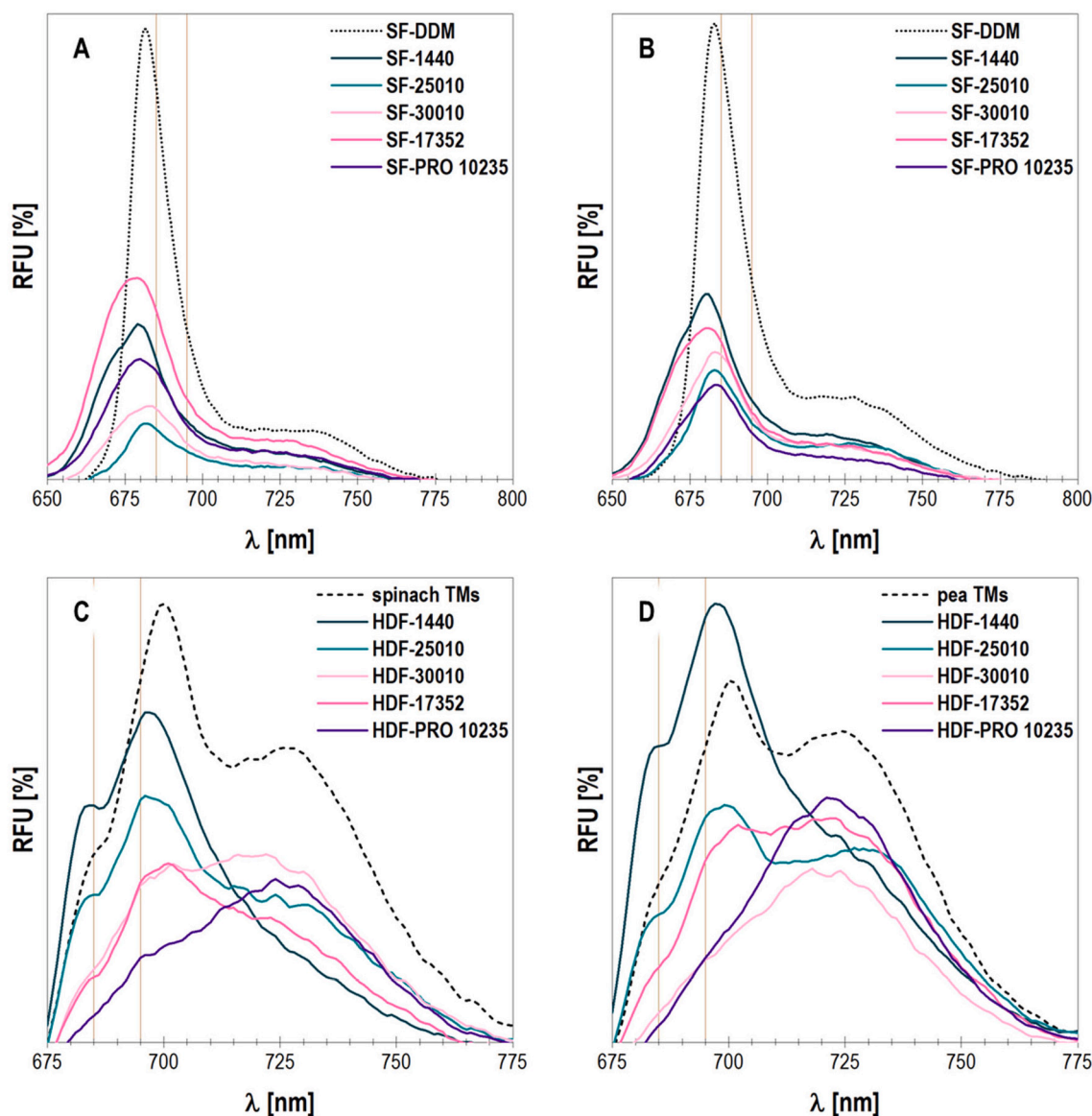


Fig. 6. Association of LHCII trimers with PSI and PSII complexes: chlorophyll fluorescence emission spectra at 77 K of solubilized spinach (A) and pea (B) thylakoid fractions and spinach (C) and pea (D) HDF-SMALPs. The reference lines at 685 and 695 nm are shown as light red solid lines. Samples were diluted in GKRB-150 with pH 9.0 to 4 $\mu\text{g}/\text{mL}$ (A and B) and 5 $\mu\text{g}/\text{mL}$ (C and D).

against PsbR, and PsbW cross-reacted neither with spinach nor with pea samples, while PsbQ had a low cross-reactivity against spinach samples.

The near total removal of the extrinsic OEC subunits (PsbO, PsbP, and PsbQ) is possibly not surprising considering the chemistry of this treatment and the mode of OEC association with PSII core subunits. The interaction of PsbO with the PSII core is largely mediated by interactions between highly conserved acidic residues, including a central motif D/E167 to D/E194 and a C-terminal region of E225 to D339 [45]. Many of these residues are easily modified using 1-ethyl-3-(3-dimethylamino-propyl)carbodiimide (EDC) [46]. Upon covalent modification with EDC, the modified PsbO lost affinity for PSII and greatly reduced levels of oxygen evolution [47]. This role of carboxyl containing amino acids for binding was confirmed by site directed mutagenesis [48,49] where changing of D to A reduced binding of PsbO to PSII. Moreover, it has been known for a long time that washing of thylakoids with solutions containing high (~ 250 mM NaCl) salt concentrations will inhibit oxygen evolution and largely remove the extrinsic subunits: PsbP and PsbQ [50]. Treatment of the thylakoids with alkaline buffers with pH ~ 9.8 also resulted in total loss of the PsbO, PsbP, and PsbQ subunits [50].

PsbO is bound to PSII by electrostatic and hydrogen bonding forces. The SMA polymer salts all have a high carboxylic acid content indicated by the maleic acid content as shown in Table II. It is possible that the insertion of the SMA copolymer is able to displace the OEC subunits by replacing the key carboxylate groups responsible for OEC binding to the core. It is also possible that the high pH (pH ~ 10) used in the thylakoid washing with Na_2CO_3 may have removed or partially weakened this interaction prior to solubilization step with SMA copolymer, yet these washed thylakoids still show the presence of these subunits.

Generally, HDF-1440, HDF-25010, and HDF-17352 are enriched in Lhcb1–6, while HDF-30010 and HDF-PRO 10235 are depleted in Lhcb5 and Lhcb6. This result combined with the previous data suggest that LHCII trimer (M) did not get solubilized together with PSII by SMA polymers 30010 and PRO 10235. All HDF-SMALPs are enriched in PsbA, PsbB, and PsbD. This indicates the presence of PSI and PSII core reaction centers in HDF-SMALPs. Thus, based on the results we can conclude that PSI, PSII, and LHCII are present in HDF-SMALPs, probably as a mixture of PSI–LHCII and PSII–LHCII supramolecular protein complexes.

Table III

Deconvolution results of fluorescence emission spectra: peak maximum and area ratio. The values are color-coded with the white/yellow color corresponding to the lowest value and the red/green – to the highest value.

species	HDF-SMALP	λ_{\max} [nm]		Peak area [counts]		A_3/A_2
		peak 2	peak 3	A_2	A_3	[a.u.]
spinach	HDF-PRO 10235	696.0	724.6	12910 ± 782	131302 ± 139	10.2 ± 0.6
	HDF-30010	696.2	720.3	22779 ± 1754	174944 ± 2140	7.7 ± 0.7
	TM	698.4	725.0	98623 ± 2207	246197 ± 5003	2.5 ± 0.1
	HDF-17352	698.0	720.9	45849 ± 3283	99401 ± 3576	2.2 ± 0.2
	HDF-25010	696.0	723.7	74656 ± 2886	133099 ± 2927	1.8 ± 0.1
	HDF-1440	695.7	716.1	114350 ± 10677	96710 ± 11036	0.8 ± 0.2
pea	HDF-PRO 10235	695.3	722.4	2039 ± 477	195216 ± 217	95.7 ± 22.5
	HDF-30010	698.0	721.3	7391 ± 2583	141010 ± 2984	19.1 ± 7.1
	HDF-17352	697.6	722.0	36011 ± 1919	194470 ± 2228	5.4 ± 0.3
	TM	698.1	723.3	69755 ± 2451	265094 ± 2448	3.8 ± 0.2
	HDF-25010	696.6	727.2	72490 ± 1610	164969 ± 1491	2.3 ± 0.1
	HDF-1440	695.9	718.0	123864 ± 5033	204781 ± 5877	1.7 ± 0.1

Recently, there has been considerable progress in elucidating the structure and function of the light harvesting complexes associated with PSI and PSII [51–53]. Following extraction with SMA copolymers, the antennae complexes (LHCII and possibly LHCI) associated with the supramolecular membrane proteins appeared to be energetically coupled to PSII and possibly PSI based on 77 K chlorophyll fluorescence emission spectroscopy study. The estimated ratio of PSI-to-PSII/LHCII in the HDF-SMALPs varies for both spinach and pea samples, and decreases depending on the type of SMA copolymer in the following order: HDF-PRO 10235 > HDF-30010 > HDF-17352 > HDF-25010 > HDF-1440. The chlorophyll *a/b* mole ratio increases in the series HDF-1440 < HDF-25010 < HDF-17352 ≈ HDF-30010 < HDF-PRO 10235 ranging from 1.7 ± 0.1 to 3.4 ± 0.5 . The high chlorophyll *a/b* ratio for HDF-PRO 10235, combined with the high A_3/A_2 ratio, suggest that the SMA copolymer PRO 10235 predominantly extracts a highly coupled LHCI-PSI supramolecular complex. Future work will need to be done to investigate the structure and function of the multiple Lhca subunits associated with PSI especially in light of how variable these complexes can be depending on growth conditions [54].

It has been reported that in green algae the number of Lhca subunits can vary from 7 in *Dunaliella* [55] to ~10 in *Chlamydomonas* [56] and *Bryopsis* [57]. In *Chlamydomonas*, two types of supercomplexes have been observed and are referred to as PSI – 8 LHCI and PSI – 10 LHCI. In PSI – 8 LHCI the eight LHCI complexes are organized in two layers at one side of the PSI core outside of where the Psf is located. Each layer contains four LHCI complexes arranged in an arc, forming an inner and outer LHCI belt [54]. It would appear that in some algae there is also the ability to form an unusual Lhca dimer [57]. However, it is also believed the algae have a larger and more diverse antenna organization that enables a higher light-harvesting capability than what has been observed thus far in land plants with only four Lhca subunits observed in pea [58,59]. Possibly the other Lhca subunits are lost during detergent solubilization. Interestingly, Psf also seems to be lost in these higher plant PSI – SMALP complexes (Fig. 6C) as was reported earlier in the SMA isolation of cyanobacterial trimeric PSI complexes [18,60].

Although we still lack a high-resolution structure of the LHCII-PSII core structure we know that this complex can exist in different oligomeric forms from the minimal C_2S_2 up to the much larger $C_2S_2M_2$ [61–64], where C is for the core PSII dimer that has a two-fold access of symmetry, and the S and M represent different trimeric LHCII complexes that flank the core complex. These S and M trimers are composed of Lhcb1–3 subunits in different ratios depending on light levels. However,

from combining a structural model with recent chemical crosslinking and proteomics [65,66] we now have a fairly good model of the pea LHCII – PSII supramolecular complex, which is shown schematically in Fig. S9. The work investigated the composition of these complexes in pea plants grown under different light levels. It was evident that main light-dependent variability is in the composition of the LHCII subunits associated with these larger supramolecular complexes.

Extraction of HDF-SMALPs of varied composition with different derivatives of SMA polymers may be a subtle way of identifying these different LHCII – PSI assemblies. For example, our immunoblotting results reveals a clear difference in Lhcb subunit composition of the pea and spinach HDF-SMALPs using different SMA copolymers (Fig. 7A and B). Although not quantitative, all five SMA copolymers tested show strong reactivity with the antibodies against Lhcb1, Lhcb2, and Lhcb3. Lhcb1 emerged as the most abundant LHCII component, with intensity levels at least two-fold higher than Lhcb2 and Lhcb3 with all SMA copolymers. This is interesting since all three of these Lhcb subunits are all assembled into the heterotrimeric complexes, S and M. However, solubilization using two of the SMA polymers (30010 and PRO 10235) produces an HDF with considerably reduced levels of Lhcb4, Lhcb5, and Lhcb6 in both pea and spinach. Unfortunately, the α -Lhcb6 antisera used does not show strong cross-reactivity in pea thylakoids with Lhcb6 being undetectable following isolation with 30010 and PRO 10235. Due to the high sequence similarity cross-reactivity between the isoforms using antibodies is a concern and the future proteomic analysis of these distinct complexes will be needed to verify these observations in more detail. However, these results would reveal that the monomeric Lhcb subunits (Lhcb4, Lhcb5, and Lhcb6) are more labile and/or in some type of rapid equilibrium that makes the solubilization with SMA polymers able to capture a smaller, truncated, or core complexes. The different supramolecular complexes from HDF-SMALPs are as a group enriched in LHCII, PSII, and PSI to different extents depending on the polymer modification. However, in all cases the HDF-SMALPs do not appear to include the cytochrome b_6/f complex which has been observed to form supramolecular complexes with PSI previously (Fig. 6D) [67,68]. Similar to the use of amphipols [69], the use of SMA copolymers may be a good method to isolate larger and more intact thylakoid supramolecular complexes which may be stabilized by the native lipids in these complexes [70].

4. Summary

We have described an efficient, one-step method for the extraction of supramolecular protein complexes from spinach and pea TMs isolated from intact chloroplasts. The described method is not limited to pea or spinach thylakoids and could be applicable to other galactolipid-rich membranes such as the thylakoids from all oxygenic organisms including cyanobacteria, algae, and all vascular plants. In addition, these methods may also be applicable to membranes from other photosynthetic prokaryotes such as *Chloroflexus* [71] and even the non-photosynthetic members of the Apicomplexa [72], whose membranes have been shown to contain galactolipids.

The composition of HDF-SMALPs separated by sucrose density gradient ultracentrifugation was experimentally studied using UV-vis spectroscopy, chlorophyll fluorescence emission spectroscopy at 77 K, gel electrophoresis, and immunoblot analysis with 22 antibodies against subunits of major thylakoid MPCs. We showed that the efficacy of SMA copolymers in membrane protein extraction depends on the intrinsic properties of the starting thylakoid membrane and on the polymer structure. The difference in thylakoid organization studied by TEM, particularly in the number of stacks per grana and the grana thickness, indicates that the spinach thylakoids contain more grana than lamellae regions. Thus, the higher solubilization efficacy, based on the efficacy of both protein and chlorophyll extraction, of the pea TMs can be explained by increased membrane fluidity due to higher surface area, lower protein-to-lipid ratio, and lateral pressure due to presence of higher

rapid speed of this separation may allow some of the highly dynamic processes associated with chloroplast membranes such as intermediates in state transitions [92] and the zeaxanthin cycle [93], plastid development/greening [94], PSII repair/degradation [95], protein trafficking [96,97], and other membrane remodeling processes [98,99] to be studied at a new level of in vitro resolution.

Funding sources

Support for BDB has been provided from the Gibson Family Foundation, the Dr. Donald L. Akers Faculty Enrichment Fellowship, and National Science Foundation (EPS-1004083). OIK, TTN, and BDB have been supported via a Joint Directed Research Development Award from University of Tennessee at Knoxville/Oak Ridge National Laboratory Science Alliance to BDB. The JEM 1400 high contrast TEM was purchased via an NSF MRI (MRI-1828300) to BDB and TMB-S. BCR and TMB-S were supported from an NSF Award (MCB-1846245) to TMB-S.

Declaration of competing interest

The authors declare that they have no known competing financial interests or personal relationships that could have appeared to influence the work reported in this paper.

Acknowledgments

Authors thank Frank Fan at PhytoAB Inc. (USA, CA, San Jose) for providing the antibodies for testing; Dr. John Dunlap for his assistance with sample preparation for electron microscopy; Maddie Davis for proofreading the manuscript and her valuable suggestions; and Aleksandra Noras for helping fractionating and analyzing sucrose density gradients.

Appendix A. Supplementary data

Supplementary data to this article can be found online at <https://doi.org/10.1016/j.bbabo.2020.148347>.

References

- C. Pagliano, S. Barera, F. Chimirri, G. Saracco, J. Barber, Comparison of the α and β isomeric forms of the detergent *n*-dodecyl-D-maltoside for solubilizing photosynthetic complexes from pea thylakoid membranes, *Biochim. Biophys. Acta Bioenerg.* 1817 (2012) 1506–1515, <https://doi.org/10.1016/j.BBABIO.2011.11.001>.
- D.J.K. Swainsbury, S. Scheidelaar, R. van Grondelle, J.A. Killian, M.R. Jones, Bacterial reaction centers purified with styrene maleic acid copolymer retain native membrane functional properties and display enhanced stability, *Angew. Chemie Int. Ed.* 53 (2014) 11803–11807, <https://doi.org/10.1002/anie.201406412>.
- L.I. Osipow, Surface chemistry: theory and industrial applications. American Chemical Society. Monograph series, no. 153, in: *Surf. Chem. Theory Ind. Appl.*, Reinhold Publishing Corporation, New York, 1962, p. 473. https://books.google.com/books/about/Surface_Chemistry.html?id=uozcuQEACAAJ.
- M. Overduin, M. Esmaili, Structures and Interactions of Transmembrane Targets in Native Nanodiscs, *SLAS Discov.* 2019, <https://doi.org/10.1177/2472555219857691>.
- M. Overduin, M. Esmaili, Native nanodiscs and the convergence of lipidomics, metabolomics, interactomics and proteomics, *Appl. Sci.* 9 (2019) 1230, <https://doi.org/10.3390/app9061230>.
- M. Overduin, M. Esmaili, Memtein: the fundamental unit of membrane-protein structure and function, *Chem. Phys. Lipids* 218 (2019) 73–84, <https://doi.org/10.1016/j.chemphyslip.2018.11.008>.
- M. Overduin, B. Klumperman, Advancing membrane biology with poly(styrene-co-maleic acid)-based native nanodiscs, *Eur. Polym. J.* 110 (2019) 63–68, <https://doi.org/10.1016/j.eurpolymj.2018.11.015>.
- B. Andersson, J.M. Anderson, Lateral heterogeneity in the distribution of chlorophyll-protein complexes of the thylakoid membranes of spinach chloroplasts, *Biochim. Biophys. Acta Bioenerg.* 593 (1980) 427–440, [https://doi.org/10.1016/0005-2728\(80\)90078-X](https://doi.org/10.1016/0005-2728(80)90078-X).
- J.M. Anderson, Changing concepts about the distribution of photosystems I and II between grana-appressed and stroma-exposed thylakoid membranes, *Photosynth. Res.* 73 (2002) 157–164, <https://doi.org/10.1023/A:1020426525648>.
- J.M. Anderson, Lateral heterogeneity of plant thylakoid protein complexes: early reminiscences, *Philos. Trans. R. Soc. B Biol. Sci.* 367 (2012) 3384–3388, <https://doi.org/10.1098/rstb.2012.0060>.
- A. Strašková, G. Steinbach, G. Konert, E. Kotabová, J. Komenda, M. Tichý, R. Kaňa, Pigment-protein complexes are organized into stable microdomains in cyanobacterial thylakoids, *Biochim. Biophys. Acta Bioenerg.* 2019 (1860), <https://doi.org/10.1016/j.bbabo.2019.07.008>.
- H. Koochak, S. Puthiyaveetil, D.L. Mullendore, M. Li, H. Kirchoff, The structural and functional domains of plant thylakoid membranes, *Plant J.* 97 (2019) 412–429, <https://doi.org/10.1111/tpj.14127>.
- O. Korotych, J. Mondal, K.M. Gattás-Asfura, J. Hendricks, B.D. Bruce, Evaluation of commercially available styrene-co-maleic acid polymers for the extraction of membrane proteins from spinach chloroplast thylakoids, *Eur. Polym. J.* 114 (2019) 485–500, <https://doi.org/10.1016/j.eurpolymj.2018.10.035>.
- I. Sakurai, J.-R. Shen, J. Leng, S. Ohashi, M. Kobayashi, H. Wada, Lipids in oxygen-evolving photosystem II complexes of cyanobacteria and higher plants, *J. Biochem.* 140 (2006) 201–209, <https://doi.org/10.1093/jb/mvj141>.
- L. Boudière, M. Michaud, D. Petroutsos, F. Rébeillé, D. Falconet, O. Bastien, S. Roy, G. Finazzi, N. Rolland, J. Jouhet, M.A. Block, E. Maréchal, Glycerolipids in photosynthesis: composition, synthesis and trafficking, *Biochim. Biophys. Acta Bioenerg.* 1837 (2014) 470–480, <https://doi.org/10.1016/j.BBABIO.2013.09.007>.
- M.D. Phan, O.I. Korotych, N.G. Brady, M.M. Davis, S.K. Satija, J.F. Ankner, B. D. Bruce, X-ray and neutron reflectivity studies of styrene-maleic acid copolymer interactions with galactolipid-containing monolayers, *Langmuir.* 36 (2020) 3970–3980, <https://doi.org/10.1021/acs.langmuir.9b03817>.
- A.J. Bell, L.K. Frankel, T.M. Bricker, High yield non-detergent isolation of photosystem I-light-harvesting chlorophyll II membranes from spinach thylakoids: implications for the organization of the PS I antennae in higher plants, *J. Biol. Chem.* 290 (2015) 18429–18437, <https://doi.org/10.1074/jbc.M115.663872>.
- N.G. Brady, M. Li, Y. Ma, J.C. Gumbart, B.D. Bruce, Non-detergent isolation of a cyanobacterial photosystem I using styrene maleic acid alternating copolymers, *RSC Adv.* 9 (2019) 31781–31796, <https://doi.org/10.1039/C9RA04619D>.
- N.V. Dudkina, R. Kouřil, J.B. Bultema, E.J. Boekema, Imaging of organelles by electron microscopy reveals protein-protein interactions in mitochondria and chloroplasts, *FEBS Lett.* 584 (2010) 2510–2515, <https://doi.org/10.1016/j.febslet.2010.03.027>.
- B. Daum, W. Kuhlbrandt, Electron tomography of plant thylakoid membranes, *J. Exp. Bot.* 62 (2011) 2393–2402, <https://doi.org/10.1093/jxb/err034>.
- B.D. Engel, M. Schaffer, L. Kuhn Cuellar, E. Villa, J.M. Plitzko, W. Baumeister, Native architecture of the *Chlamydomonas* chloroplast revealed by *in situ* cryo-electron tomography, *Elife* 4 (2015), <https://doi.org/10.7554/eLife.04889>.
- X. Pi, L. Tian, H.-E. Dai, X. Qin, L. Cheng, T. Kuang, S.-F. Sui, J.-R. Shen, Unique organization of photosystem I-light-harvesting supercomplex revealed by cryo-EM from a red alga, *Proc. Natl. Acad. Sci.* 115 (2018) 4423–4428, <https://doi.org/10.1073/pnas.1722482115>.
- M. Iwai, P. Grob, A.T. Iavarone, E. Nogales, K.K. Niyogi, A unique supramolecular organization of photosystem I in the moss *Physcomitrella patens*, *Nat. Plants.* 4 (2018) 904–909, <https://doi.org/10.1038/s41477-018-0271-1>.
- R.N. Burton-Smith, A. Watanabe, R. Tokutsu, C. Song, K. Murata, J. Minagawa, Structural determination of the large photosystem II-light harvesting complex II supercomplex of *Chlamydomonas reinhardtii* using non-ionic amphipol, *J. Biol. Chem.* (2019), <https://doi.org/10.1074/jbc.ra119.009341>.
- H. Kirchoff, Structure-function relationships in photosynthetic membranes: challenges and emerging fields, *Plant Sci.* 266 (2018) 76–82, <https://doi.org/10.1016/j.plantsci.2017.09.021>.
- H. Kaczmarek, A. Felczak, A. Szalla, Studies of photochemical transformations in polystyrene and styrene-maleic anhydride copolymer, *Polym. Degrad. Stab.* 93 (2008) 1259–1266, <https://doi.org/10.1016/j.polyimdegradstab.2008.04.011>.
- B.D. Bruce, S. Perry, J. Froehlich, K. Keegstra, *In vitro* import of proteins into chloroplasts, in: S.B. Gelvin, R.A. Schilperoot (Eds.), *Plant Mol. Biol. Man.*, Springer Netherlands, Dordrecht, 1994, pp. 497–511, https://doi.org/10.1007/978-94-011-0511-8_32.
- Y. Fujiki, A.L. Hubbard, S. Fowler, P.B. Lazarow, Isolation of intracellular membranes by means of sodium carbonate treatment: application to endoplasmic reticulum, *J. Cell Biol.* 93 (1982) 97–102. <http://www.ncbi.nlm.nih.gov/pubmed/7068762>. (Accessed 31 May 2018).
- K. Bobik, J.R. Dunlap, T.M. Burch-Smith, Tandem high-pressure freezing and quick freeze substitution of plant tissues for transmission electron microscopy, *J. Vis. Exp.* (2014) 1–10, <https://doi.org/10.3791/51844>.
- J. Schindelin, I. Arganda-Carreras, E. Frise, V. Kaynig, M. Longair, T. Pietzsch, S. Preibisch, C. Rueden, S. Saalfeld, B. Schmid, J.-Y. Tinevez, D.J. White, V. Hartenstein, K. Eliceiri, P. Tomancak, A. Cardona, Fiji: an open-source platform for biological-image analysis, *Nat. Methods* 9 (2012) 676–682, <https://doi.org/10.1038/nmeth.2019>.
- R.J. Porra, W.A. Thompson, P.E. Kriedemann, Determination of accurate extinction coefficients and simultaneous equations for assaying chlorophylls a and b extracted with four different solvents: verification of the concentration of chlorophyll standards by atomic absorption spectroscopy, *Biochim. Biophys. Acta Bioenerg.* 975 (1989) 384–394, [https://doi.org/10.1016/S0005-2728\(89\)80347-0](https://doi.org/10.1016/S0005-2728(89)80347-0).
- U.K. Laemmli, Cleavage of structural proteins during the assembly of the head of bacteriophage T4, *Nature.* 227 (1970) 680–685, <https://doi.org/10.1038/227680a0>.
- H. Schägger, Tricine-SDS-PAGE, *Nat. Protoc.* 1 (2006) 16–22, <https://doi.org/10.1038/nprot.2006.4>.
- H. Towbin, T. Staehelin, J. Gordon, Electrophoretic transfer of proteins from polyacrylamide gels to nitrocellulose sheets: procedure and some applications,

- Proc. Natl. Acad. Sci. U. S. A. 76 (1979) 4350–4354. <http://www.ncbi.nlm.nih.gov/pubmed/388439>. (Accessed 8 November 2018).
- [35] B.N. Taylor, C.E. Kuyatt, Guidelines for evaluating and expressing the uncertainty of NIST measurement results, NIST Tech. Note. 1297 (1994) 20.
- [36] S. Barera, C. Pagliano, T. Pape, G. Saracco, J. Barber, Characterization of PSII-LHCII supercomplexes isolated from pea thylakoid membrane by one-step treatment with α - and β -dodecyl- α -D-maltoside and expressing the uncertainty of NIST measurement results, NIST Tech. Note. 1297 (1994) 20.
- [37] S. Scheidelaar, M.C. Koorengel, J.D. Pardo, J.D. Meeldijk, E. Breukink, J. A. Killian, Molecular model for the solubilization of membranes into nanodisks by styrene maleic acid copolymers, Biophys. J. 108 (2015) 279–290, <https://doi.org/10.1016/j.bpj.2014.11.3464>.
- [38] A.A. Gulamhussein, D. Meah, D.D. Soja, S. Fenner, Z. Saidani, A. Akram, S. Lallie, A. Mathews, C. Painter, M.K. Liddar, Z. Mohammed, L.K. Chiu, S.S. Sumar, H. Healy, N. Hussain, J.H. Patel, S.C.L. Hall, T.R. Dafforn, A.J. Rothnie, Examining the stability of membrane proteins within SMALPs, Eur. Polym. J. 112 (2019) 120–125, <https://doi.org/10.1016/j.eurpolymj.2018.12.008>.
- [39] J.W.M. Heemskerk, T. Storz, R.R. Schmidt, E. Heinz, Biosynthesis of Digalactosyldiacylglycerol in Plastids from 16:3 and 18:3 Plants, 1990.
- [40] D.J. Chapman, J. De-Felice, J. Barber, Growth temperature effects on thylakoid membrane lipid and protein content of pea chloroplasts, Plant Physiol. 72 (1983) 225–228, <https://doi.org/10.1104/pp.72.1.225>.
- [41] X. Pan, P. Cao, X. Su, Z. Liu, M. Li, Structural analysis and comparison of light-harvesting complexes I and II, Biochim. Biophys. Acta Bioenerg. 2020 (1861) 148038, <https://doi.org/10.1016/j.bbabi.2019.06.010>.
- [42] R. Croce, H. van Amerongen, Light-harvesting in photosystem I, Photosynth. Res. 116 (2013) 153–166, <https://doi.org/10.1007/s1120-013-9838-x>.
- [43] L. Nosek, D. Semchonok, E.J. Boekema, P. Ilík, R. Kouril, Structural variability of plant photosystem II megacomplexes in thylakoid membranes, Plant J. 89 (2017) 104–111, <https://doi.org/10.1111/tpj.13325>.
- [44] J.J. Lamb, G. Røkke, M.F. Hohmann-Mariott, Chlorophyll fluorescence emission spectroscopy of oxygenic organisms at 77 K, Photosynthetica. 56 (2018) 105–124, <https://doi.org/10.1007/s11099-018-0791-y>.
- [45] T.M. Bricker, R.L. Burnap, The extrinsic proteins of photosystem II, in: Photosyst. II, Springer-Verlag, Berlin/Heidelberg, 2006, pp. 95–120, https://doi.org/10.1007/1-4020-4254-X_6.
- [46] A. Seidler, Intermolecular and intramolecular interactions of the 33-kDa protein in photosystem II, Eur. J. Biochem. 242 (1996) 485–490, <https://doi.org/10.1111/j.1432-1033.1996.0485r.x>.
- [47] L.K. Frankel, J.A. Cruz, T.M. Bricker, Carboxylate groups on the manganese-stabilizing protein are required for its efficient binding to photosystem II, Biochemistry. 38 (1999) 14271–14278, <https://doi.org/10.1021/bi991366v>.
- [48] A. Seidler, The extrinsic polypeptides of photosystem II, Biochim. Biophys. Acta Bioenerg. 1277 (1996) 35–60, [https://doi.org/10.1016/S0005-2728\(96\)00102-8](https://doi.org/10.1016/S0005-2728(96)00102-8).
- [49] R.L. Burnap, M. Qian, J.-R. Shen, Y. Inoue, L.A. Sherman, Role of disulfide linkage and putative intermolecular binding residues in the stability and binding of the extrinsic manganese-stabilizing protein to the photosystem II reaction center, Biochemistry. 33 (1994) 13712–13718, <https://doi.org/10.1021/bi00250a023>.
- [50] M. Beauregard, L. Morin, R. Popovic, Removal of the 33, 23 and 18 kDa extrinsic proteins of photosystem II by sulfite treatment at alkaline pH, Biochem. Biophys. Res. Commun. 152 (1988) 612–616, [https://doi.org/10.1016/S0006-291X\(88\)80082-2](https://doi.org/10.1016/S0006-291X(88)80082-2).
- [51] X. Pan, J. Ma, X. Su, P. Cao, W. Chang, Z. Liu, X. Zhang, M. Li, Structure of the maize photosystem I supercomplex with light-harvesting complexes I and II, Science (80-) 360 (2018) 1109–1113, <https://doi.org/10.1126/science.aat1156>.
- [52] A. Crepin, Z. Kucerova, A. Kosta, E. Durand, S. Caffarri, Isolation and characterization of a large photosystem I-light-harvesting complex II supercomplex with an additional Lhca1-a4 dimer in Arabidopsis, Plant J 102 (2) (2020) 398–409, <https://doi.org/10.1111/tpj.14634>.
- [53] J. Gao, H. Wang, Q. Yuan, Y. Feng, Structure and function of the photosystem supercomplexes, Front. Plant Sci. 9 (2018) 357, <https://doi.org/10.3389/fpls.2018.00357>.
- [54] M. Suga, J.-R. Shen, Structural variations of photosystem I-antenna supercomplex in response to adaptations to different light environments, Curr. Opin. Struct. Biol. 63 (2020) 10–17, <https://doi.org/10.1016/j.sbi.2020.02.005>.
- [55] A. Perez-Boerema, D. Klaiman, I. Caspy, S.Y. Netzer-El, A. Amunts, N. Nelson, Structure of a minimal photosystem I from the green alga *Dunaliella salina*, Nat. Plants. 6 (2020) 321–327, <https://doi.org/10.1038/s41477-020-0611-9>.
- [56] M. Suga, S.-I. Ozawa, K. Yoshida-Motomura, F. Akita, N. Miyazaki, Y. Takahashi, Structure of the green algal photosystem I supercomplex with a decameric light-harvesting complex I, Nat. Plants. 5 (2019) 626–636, <https://doi.org/10.1038/s41477-019-0438-4>.
- [57] X. Qin, X. Pi, W. Wang, G. Han, L. Zhu, M. Liu, L. Cheng, J.-R. Shen, T. Kuang, S.-F. Sui, Structure of a green algal photosystem I in complex with a large number of light-harvesting complex I subunits, Nat. Plants. 5 (2019) 263–272, <https://doi.org/10.1038/s41477-019-0379-y>.
- [58] Y. Mazor, A. Borovikova, I. Caspy, N. Nelson, Structure of the plant photosystem I supercomplex at 2.6 Å resolution, Nat. Plants 3 (2017) 17014, <https://doi.org/10.1038/nplants.2017.14>.
- [59] H. Kubota-Kawai, R.N. Burton-Smith, R. Tokutsu, C. Song, S. Akimoto, M. Yokono, Y. Ueno, E. Kim, A. Watanabe, K. Murata, J. Minagawa, Ten antenna proteins are associated with the core in the supramolecular organization of the photosystem I supercomplex in *Chlamydomonas reinhardtii*, J. Biol. Chem. 294 (2019) 4304–4314, <https://doi.org/10.1074/jbc.RA118.006536>.
- [60] D.A. Cherepanov, N.G. Brady, I.V. Shelaev, J. Nguyen, F.E. Gostev, M.D. Mamedov, V.A. Nadtchenko, B.D. Bruce, PSI-SMALP, a detergent-free cyanobacterial photosystem I, reveals faster femtosecond photochemistry, Biophys. J. 118 (2020) 337–351, <https://doi.org/10.1016/j.bpj.2019.11.3391>.
- [61] P. Albanese, J. Nield, J.A.M. Tabares, A. Chiodoni, M. Manfredi, F. Gosetti, E. Marengo, G. Saracco, J. Barber, C. Pagliano, Isolation of novel PSII-LHCII megacomplexes from pea plants characterized by a combination of proteomics and electron microscopy, Photosynth. Res. 130 (2016) 19–31, <https://doi.org/10.1007/s1120-016-0216-3>.
- [62] X. Sheng, A. Watanabe, A. Li, E. Kim, C. Song, K. Murata, D. Song, J. Minagawa, Z. Liu, Structural insight into light harvesting for photosystem II in green algae, Nat. Plants. 5 (2019) 1320–1330, <https://doi.org/10.1038/s41477-019-0543-4>.
- [63] L. Shen, Z. Huang, S. Chang, W. Wang, J. Wang, T. Kuang, G. Han, J.-R. Shen, X. Zhang, Structure of a C₂S₂M₂N₂-type PSII-LHCII supercomplex from the green alga *Chlamydomonas reinhardtii*, Proc. Natl. Acad. Sci. 116 (2019) 21246–21255, <https://doi.org/10.1073/pnas.1912462116>.
- [64] X. Su, J. Ma, X. Wei, P. Cao, D. Zhu, W. Chang, Z. Liu, X. Zhang, M. Li, Structure and assembly mechanism of plant C₂S₂M₂-type PSII-LHCII supercomplex, Science (80-) 357 (2017) 815–820, <https://doi.org/10.1126/science.aan0327>.
- [65] P. Albanese, R. Melero, B.D. Engel, A. Grinzato, P. Berto, M. Manfredi, A. Chiodoni, J. Vargas, C.O.S. Sorzano, E. Marengo, G. Saracco, G. Zanotti, J.-M. Carazo, C. Pagliano, Pea PSII-LHCII supercomplexes form pairs by making connections across the stromal gap, Sci. Rep. 7 (2017) 10067, <https://doi.org/10.1038/s41598-017-10700-8>.
- [66] P. Albanese, S. Tamara, G. Saracco, R.A. Scheltema, C. Pagliano, How paired PSII-LHCII supercomplexes mediate the stacking of plant thylakoid membranes unveiled by structural mass-spectrometry, Nat. Commun. 11 (2020) 1361, <https://doi.org/10.1038/s41467-020-15184-1>.
- [67] K.N.S. Yadav, D.A. Semchonok, L. Nosek, R. Kouril, G. Fucile, E.J. Boekema, L. A. Eichacker, Supercomplexes of plant photosystem I with cytochrome b₆/f, light-harvesting complex II and NDH, Biochim. Biophys. Acta Bioenerg. 1858 (2017) 12–20, <https://doi.org/10.1016/j.bbabi.2016.10.006>.
- [68] J. Steinbeck, I.L. Ross, R. Rothnagel, P. Gäbelein, S. Schulze, N. Giles, R. Ali, R. Drysdale, E. Sierceki, Y. Gambin, H. Stahlberg, Y. Takahashi, M. Hippler, B. Hankamer, Structure of a PSI-LHCI-cyt b₆/f supercomplex in *Chlamydomonas reinhardtii* promoting cyclic electron flow under anaerobic conditions, Proc. Natl. Acad. Sci. 115 (2018) 10517–10522, <https://doi.org/10.1073/pnas.1809973115>.
- [69] A. Watanabe, E. Kim, R.N. Burton-Smith, R. Tokutsu, J. Minagawa, Amphipol-assisted purification method for the highly active and stable photosystem II supercomplex of *Chlamydomonas reinhardtii*, FEBS Lett. 593 (2019) 1072–1079, <https://doi.org/10.1002/1873-3468.13394>.
- [70] X. Sheng, X. Liu, P. Cao, M. Li, Z. Liu, Structural roles of lipid molecules in the assembly of plant PSII-LHCII supercomplex, Biophys. Reports. 4 (2018) 189–203, <https://doi.org/10.1007/s41048-018-0068-9>.
- [71] C.N. Kenyon, A.M. Gray, Preliminary Analysis of Lipids and Fatty Acids of Green Bacteria and *Chloroflexus aurantiacus*, 1974.
- [72] E. Maréchal, N. Azzouz, C. Santos de Macedo, M.A. Block, J.E. Feagin, R. T. Schwarz, J. Joyard, Synthesis of chloroplast galactolipids in Apicomplexan parasites, Eukaryot. Cell 1 (2002) 653–656, <https://doi.org/10.1128/EC.1.4.653-656.2002>.
- [73] D.G. Carneiro, T. Clarke, C.C. Davies, D. Bailey, Identifying novel protein interactions: proteomic methods, optimisation approaches and data analysis pipelines, Methods. 95 (2016) 46–54, <https://doi.org/10.1016/j.ymeth.2015.08.022>.
- [74] M. Rantala, V. Paakkari, E.-M. Aro, Analysis of thylakoid membrane protein complexes by blue native gel electrophoresis, J. Vis. Exp. 2018 (2018), <https://doi.org/10.3791/58369>.
- [75] N.L. Pollock, M. Rai, K.S. Simon, S.J. Hesketh, A.C.K. Teo, M. Parnar, P. Sridhar, R. Collins, S.C. Lee, Z.N. Stroud, S.E. Bakker, S.P. Muench, C.H. Barton, G. Hurlbut, D.I. Roper, C.J.I. Smith, T.J. Knowles, C.M. Spickett, J.M. East, V.L.G. Postis, T. R. Dafforn, SMA-PAGE: a new method to examine complexes of membrane proteins using SMALP nano-encapsulation and native gel electrophoresis, Biochim. Biophys. Acta Biomembr. 1861 (2019) 1437–1445, <https://doi.org/10.1016/j.bbame.2019.05.011>.
- [76] A. Linden, M. Deckers, I. Parfentev, R. Pflanz, B. Homberg, P. Neumann, R. Ficner, P. Rehling, H. Urlaub, A cross-linking mass spectrometry approach defines protein interactions in yeast mitochondria, Mol. Cell. Proteomics. (2020), <https://doi.org/10.1074/mcp.RA120.002028>.
- [77] S.N. Lomin, G.A. Romanov, A new tool for quantification of membrane protein partitioning between different cell membranes, Anal. Biochem. 599 (2020) 113734, <https://doi.org/10.1016/j.ab.2020.113734>.
- [78] C.A.S. Banks, S.E. Kong, M.P. Washburn, Affinity purification of protein complexes for analysis by multidimensional protein identification technology, Protein Expr. Purif. 86 (2012) 105–119, <https://doi.org/10.1016/j.pep.2012.09.007>.
- [79] F.L. Conlon, Y. Miteva, E. Kaltenbrun, L. Waldron, T.M. Greco, I.M. Cristea, Immunoprecipitation of protein complexes from *Xenopus*, in: Methods Mol. Biol., NIH Public Access, 2012, pp. 369–390, https://doi.org/10.1007/978-1-61779-992-1_21.
- [80] M. Kumar, R. Singh, A. Meena, B.S. Patidar, R. Prasad, S.K. Chhabra, S.K. Bansal, An improved 2-dimensional gel electrophoresis method for resolving human erythrocyte membrane proteins, Proteomics Insights. 8 (2017), <https://doi.org/10.1177/1178641817700880>, 1178641817700880.
- [81] G. Smejkal, S. Kakumantu, Two-Dimensional 16-BAC/SDS Polyacrylamide Gel Electrophoresis of Mitochondrial Membrane Proteins, in: Methods Mol. Humana Press Inc., Biol, 2019, pp. 55–68, https://doi.org/10.1007/978-1-4939-8814-3_3.
- [82] J.F. Bada Juarez, A.J. Harper, P.J. Judge, S.R. Tonge, A. Watts, From polymer chemistry to structural biology: the development of SMA and related amphipathic

- polymers for membrane protein extraction and solubilisation, *Chem. Phys. Lipids* 221 (2019) 167–175, <https://doi.org/10.1016/j.chemphyslip.2019.03.008>.
- [83] C. Sun, R.B. Gennis, Single-particle cryo-EM studies of transmembrane proteins in SMA copolymer nanodiscs, *Chem. Phys. Lipids* 221 (2019) 114–119, <https://doi.org/10.1016/j.chemphyslip.2019.03.007>.
- [84] M. Parmar, S. Rawson, C.A. Scarff, A. Goldman, T.R. Dafforn, S.P. Muench, V.L. G. Postis, Using a SMALP platform to determine a sub-nm single particle cryo-EM membrane protein structure, *Biochim. Biophys. Acta Biomembr.* 1860 (2018) 378–383, <https://doi.org/10.1016/j.bbamem.2017.10.005>.
- [85] B. Danielczak, S. Keller, Collisional lipid exchange among DIBMA-encapsulated nanodiscs (DIBMALPs), *Eur. Polym. J.* 109 (2018) 206–213, <https://doi.org/10.1016/j.eurpolymj.2018.09.043>.
- [86] R.L. Grime, J. Goulding, R. Uddin, L.A. Stoddart, S.J. Hill, D.R. Poyner, S. J. Briddon, M. Wheatley, Single Molecule Binding of a Ligand to a G-protein-coupled Receptor in Real Time Using Fluorescence Correlation Spectroscopy, Rendered Possible by Nano-encapsulation in Styrene Maleic Acid Lipid Particles, *Nanoscale*, 2020, <https://doi.org/10.1039/D0NR01060J>.
- [87] A.J. Horsey, D.A. Briggs, N.D. Holliday, S.J. Briddon, I.D. Kerr, Application of fluorescence correlation spectroscopy to study substrate binding in styrene maleic acid lipid copolymer encapsulated ABCG2, *Biochim. Biophys. Acta Biomembr.* 2020 (1862) 183218, <https://doi.org/10.1016/j.bbamem.2020.183218>.
- [88] V. Schmidt, M. Sidore, C. Bechara, J.-P. Duneau, J.N. Sturgis, The lipid environment of *Escherichia coli* aquaporin Z, *Biochim. Biophys. Acta Biomembr.* 1861 (2019) 431–440, <https://doi.org/10.1016/j.bbamem.2018.10.017>.
- [89] I.D. Sahu, G. Dixit, W.D. Reynolds, R. Kaplevatsky, B.D. Harding, C.K. Jaycox, R. M. McCarrick, G.A. Lorigan, Characterization of the human KCNQ1 voltage sensing domain (VSD) in Lipidseq nanoparticles for electron paramagnetic resonance (EPR) spectroscopic studies of membrane proteins, *J. Phys. Chem. B* 124 (2020) 2331–2342, <https://doi.org/10.1021/acs.jpcc.9b11506>.
- [90] S.H. Park, J. Wu, Y. Yao, C. Singh, Y. Tian, F.M. Marassi, S.J. Opella, Membrane proteins in magnetically aligned phospholipid polymer discs for solid-state NMR spectroscopy, *Biochim. Biophys. Acta Biomembr.* 2020 (1862) 183333, <https://doi.org/10.1016/j.bbamem.2020.183333>.
- [91] J.S. van't Klooster, T.-Y. Cheng, H.R. Sikkema, A. Jeucken, B. Moody, B. Poolman, Periprotein lipidomes of *Saccharomyces cerevisiae* provide a flexible environment for conformational changes of membrane proteins, *Elife* 9 (2020), <https://doi.org/10.7554/eLife.57003>.
- [92] P. Longoni, I. Samol, M. Goldschmidt-Clermont, The kinase STATE TRANSITION 8 phosphorylates light harvesting complex II and contributes to light acclimation in *Arabidopsis thaliana*, *Front. Plant Sci.* 10 (2019) 1156, <https://doi.org/10.3389/fpls.2019.01156>.
- [93] J. Zhou, S. Sekatskii, R. Welc, G. Dietler, W.I. Gruszecki, The role of xanthophylls in the supramolecular organization of the photosynthetic complex LHCI in lipid membranes studied by high-resolution imaging and nanospectroscopy, *Biochim. Biophys. Acta Bioenerg.* 2020 (1861) 148117, <https://doi.org/10.1016/j.bbabi.2019.148117>.
- [94] T. Armarego-Marriott, L. Kowalewska, A. Burgos, A. Fischer, W. Thiele, A. Erban, D. Strand, S. Kahlau, A. Hertle, J. Kopka, D. Walther, Z. Reich, M.A. Schöttler, R. Bock, Highly resolved systems biology to dissect the etioplast-tocChloroplast transition in tobacco leaves, *Plant Physiol.* 180 (2019) 654–681, <https://doi.org/10.1104/pp.18.01432>.
- [95] D.A. Weisz, V.M. Johnson, D.M. Niedzwiedzki, M.K. Shinn, H. Liu, C.F. Klitzke, M. L. Gross, R.E. Blankenship, T.M. Lohman, H.B. Pakrasi, A novel chlorophyll protein complex in the repair cycle of photosystem II, *Proc. Natl. Acad. Sci.* 116 (2019) 21907–21913, <https://doi.org/10.1073/pnas.1909644116>.
- [96] V. Shanmugabalaji, V. Douet, B. Agne, F. Kessler, Affinity purification of chloroplast translocon protein complexes using the TAP tag, *J. Vis. Exp.* 2018 (2018), e58532, <https://doi.org/10.3791/58532>.
- [97] P.M. Day, K. Inoue, S.M. Theg, Chloroplast outer membrane β -barrel proteins use components of the general import apparatus, *Plant Cell* 31 (2019) 1845–1855, <https://doi.org/10.1105/tpc.19.00001>.
- [98] P.H. Lambrev, P. Akhtar, Macroorganisation and flexibility of thylakoid membranes, *Biochem. J.* 476 (2019) 2981–3018, <https://doi.org/10.1042/BCJ20190080>.
- [99] M. Rantala, S. Rantala, E.-M. Aro, Composition, phosphorylation and dynamic organization of photosynthetic protein complexes in plant thylakoid membrane, *Photochem. Photobiol. Sci.* 19 (2020) 604–619, <https://doi.org/10.1039/D0PP00025F>.